Title

Novel types of frequency filtering in the lateral perforant path projections to dentate gyrus

Journal

The Journal of Physiology, 600(16)

ISSN

0022-3751

Authors

Quintanilla, Julian

Jia, Yousheng

Lauterborn, Julie C

et al.

Publication Date

2022-08-01

DOI

10.1113/jp283012

Peer reviewed

HHS Public Access

Author manuscript

J Physiol. Author manuscript; available in PMC 2023 August 01.

Published in final edited form as:

J Physiol. 2022 August ; 600(16): 3865–3896. doi:10.1113/JP283012.

Novel types of frequency filtering in the lateral perforant path projections to dentate gyrus

Julian Quintanilla[1], **Yousheng Jia**[1], **Julie C. Lauterborn**[1], **Benedict S. Pruess**[1], **Aliza A. Le**[1], **Conor D. Cox**[1], **Christine M. Gall**[1,2], **Gary Lynch**[1,3], **Benjamin G. Gunn**[1]

[1]Departments of Anatomy & Neurobiology, University of California, Irvine, CA, USA

[2]Departments of Neurobiology & Behavior, University of California, Irvine, CA, USA

[3]Departments of Psychiatry & Human Behavior, University of California, Irvine, CA, USA

Abstract

Despite its evident importance to learning theory and models, the manner in which the lateral perforant path (LPP) transforms signals from entorhinal cortex to hippocampus is not well understood. The present studies measured synaptic responses in the dentate gyrus (DG) of adult mouse hippocampal slices during different patterns of LPP stimulation. Theta (5 Hz) stimulation produced a modest within-train facilitation that was markedly enhanced at the level of DG output. Gamma (50 Hz) activation resulted in a singular pattern with initial synaptic facilitation being followed by a progressively greater depression. DG output was absent after only two pulses. Reducing release probability with low extracellular calcium instated frequency facilitation to gamma stimulation while long-term potentiation, which increases release by LPP terminals, enhanced within-train depression. Relatedly, per terminal concentrations of VGLUT2, a vesicular glutamate transporter associated with high release probability, were much greater in the LPP than in CA3–CA1 connections. Attempts to circumvent the potent gamma filter using a series of short (three-pulse) 50 Hz trains spaced by 200 ms were only partially successful: composite responses were substantially reduced after the first burst, an effect opposite to that recorded in field CA1. The interaction between bursts was surprisingly persistent (>1.0 s). Low calcium improved throughput during theta/gamma activation but buffering of postsynaptic calcium did not. In all, presynaptic specializations relating to release probability produce an unusual but potent

Corresponding authors B. G. Gunn and G. Lynch: Gillespie Neuroscience Research Facility, 837 Health Science Road, University of California, Irvine, CA 92697, USA. bggunn16@gmail.com and ga.s.lynch@gmail.com.
Y. Jia and J. C. Lauterborn contributed equally to this work.

Author contributions

J.Q., Y.J. and B.G. designed, performed and analysed the electrophysiology recordings. J.L., A.L. and C.C. performed and analysed the immunohistochemistry. All modelling/simulation work was completed by B.P. Lesions were completed and imaged by C.G. J.Q, B.G. and G.L. contributed to the overall conception and design of the work. All authors edited the manuscript and have approved of the final version. All authors agree to be accountable for the accuracy and integrity of the work in ensuring that any related questions are appropriately investigated and resolved. All persons designated as authors qualify for authorship and all those who qualify for authorship are listed.

The peer review history is available in the Supporting information section of this article (https://doi.org/10.1113/JP283012#support-information-section).

Competing interests

Authors declare no competing interests.

Supporting information

Additional supporting information can be found online in the Supporting Information section at the end of the HTML view of the article. Supporting information files available:

type of frequency filtering in the LPP. Patterned burst input engages a different type of filter with substrates that are also likely to be located presynaptically.

Graphical Abstract

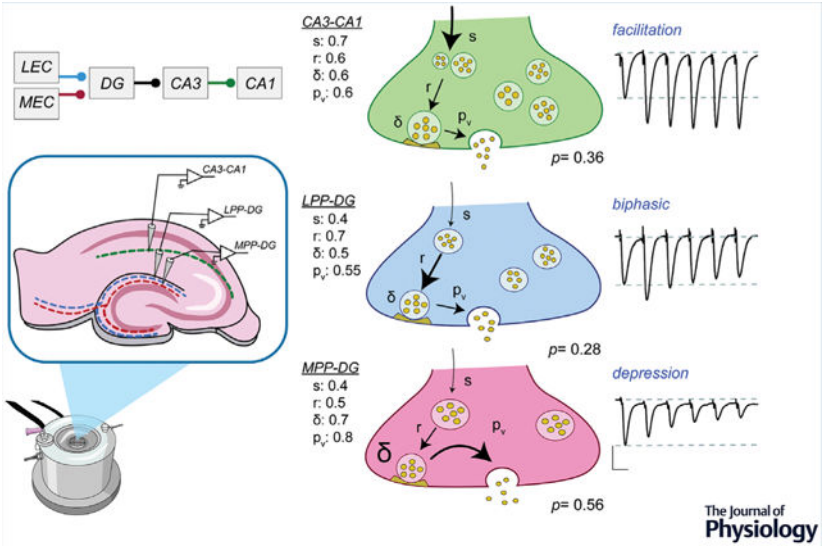

Abstract figure legend

Projections from the lateral and medial entorhinal cortex (LEC and MEC respectively) provide the primary cortical input to the hippocampus. Responses to γ frequency (50 Hz) activation differ markedly across three primary synapses of the hippocampus. While CA3–CA1 and medial perforant path (MPP)–dentate gyrus (DG) synapses display classic frequency facilitation and suppression respectively, the lateral perforant path (LPP)–DG synapse exhibits a unique biphasic output curve. Monte Carlo simulations of a two-step release model were used to test if presynaptic factors were capable of generating the distinct output curves observed at each synapse. The interaction(s) between factors within the terminal associated with vesicle release (i.e. the probability of vesicle docking (δ) and release (p_v)) and those required for vesicle recycling such as the probability of vesicles transitioning to a docked state (r) and vesicle pool replenishment (s) were found to be critical for determining the synaptic responses at each of the three synapses.

Responses to ï § frequency (50Hz) activation differ markedly across three primary synapses of the hippocampus. While CA3-CA1 and MPP-DG synapses display classic frequency facilitation and suppression respectively, the LPP-DG synapse exhibits a unique biphasic output curve. Monte Carlo simulations of a two-step release model were used to test if presynaptic factors were capable of generating the distinct output curves observed at each synapse. The interaction(s) between factors within the terminal associated with vesicle release (i.e. the probability of vesicle docking (delta symbol) and release (pv)) and those required for vesicle recycling such as the probability of vesicles transitioning to a docked state (r) and vesicle pool replenishment (s) were found to be critical for determining the synaptic responses at each of the three synapses.

Keywords

frequency facilitation; gamma oscillations; hippocampus; lateral entorhinal cortex; long-term potentiation; simulations; transmitter release; VGLUT2

Introduction

The lateral perforant path (LPP), which arises in the superficial layers of lateral entorhinal cortex, is the principal conduit through which the hippocampus receives information about cue identity (Hargreaves et al., 2005; Reagh & Yassa, 2014; Tsao et al., 2013; Witter, 1993; Yoganarasimha et al., 2011). Accordingly, the manner in which the synaptic connections formed by the projection transform (i.e. amplify, filter) incoming signals is of considerable importance for the construction of hippocampal theories and models. The entorhinal cortex–hippocampal system, along with other sites in the cortical telencephalon, typically operates at three rhythms – θ (5 Hz), β (20 Hz), and γ (>40 Hz) – during behaviour. Interleaving of θ and γ rhythms, resulting in '$\theta\gamma$' bursts, is a prominent feature of local field potentials and cell spiking during learning (Bragin et al., 1995; Chrobak & Buzsaki, 1998; Chrobak et al., 2000; Colgin, 2015; Colgin et al., 2009; Jensen & Colgin, 2007; Tort et al., 2009). Signal transformation thus involves the production of enhanced or depressed responses to repetitive inputs arriving at these frequencies or patterns. Such operations are known from work at diverse sites in the brain to require rapid adjustments on both sides of the synapse, but how they interact to produce LPP filtering is not clear.

Evidence for presynaptic modifications during repetitive stimulation was first obtained in the peripheral nervous system with the demonstration that facilitation or suppression of the second response to closely paired stimuli is dependent on initial release probability (P) (Eccles et al., 1941). Later work found that a train of afferent stimulation typically elicits frequency facilitation at those synapses showing paired pulse facilitation, whilst within-train responses progressively decrease in those synapses displaying paired pulse depression (Thomson, 2000). Considerable progress has been made in identifying presynaptic variables responsible for the two phenomena. These include mechanisms required for the mobilization and release of vesicles including Ca^{2+} entry to the terminal, detection of the cation and subsequent vesicle release, as well as those responsible for vesicle recycling and refilling (Edwards, 2007; Jackman & Regehr, 2017; Jackman et al., 2016; Nanou & Catterall, 2018). The residual Ca^{2+} hypothesis, first posited in the peripheral nervous system (Katz & Miledi, 1968), has been expanded by the identification of synaptotagmin 7 (Syt7) as a secondary high affinity, slow activating Ca^{2+} sensor in the presynaptic terminal. Genomic manipulations confirmed that Syt7 is critical for frequency facilitation in hippocampal and thalamo-cortical synapses (Jackman et al., 2016).

Complementing these findings are results showing that the type of vesicular glutamate transporter (i.e. VGLUT1 or VGLUT2) expressed at a synapse correlates with the initial release probability, a factor that as noted plays a central role in determining if contacts facilitate or depress when repetitively stimulated. The two transporters have different expression profiles within the brain (Fremeau et al., 2001) with VGLUT1 largely confined

to the cortex and VGLUT2 expressed elsewhere. Terminals with high levels of VGLUT2 depress during high rates of input while those containing VGLUT1 generally exhibit frequency facilitation. Although some evidence suggests a potential role for VGLUT isoform-specific interactions with factors governing exocytosis (Weston et al., 2011), the primary role of these proteins is in vesicle refilling (Edwards, 2007).

The CA3–CA1 (i.e. Schaffer–commissural) connections of hippocampus exhibit robust facilitation across theta to gamma frequencies (Amani et al., 2021; Trieu et al., 2015) but there are inconsistencies between reports for the LPP (Jackman et al., 2016; Wang, Jia et al., 2018). Given the significance of the issue the aim of the present study was to re-examine LPP responses elicited in the outer molecular layer (OML) of the dentate gyrus (DG) to short trains of θ, β, or γ frequency stimulation. Using electrophysiological approaches, we performed a detailed analysis of the operations occurring at the LPP–DG synapses and describe a potent form of low pass filtering. The contribution of pre- and postsynaptic factors to this LPP–DG filter, and how they may differ from the CA3–CA1 synapse was then investigated using selective pharmacological agents, immunocytochemistry, and computational approaches. Additional studies then evaluated responses to a sequence of brief γ frequency bursts (three pulses) spaced apart by the period of the θ wave (the above noted ‘theta/gamma’ bursts). A large body of work shows that such bursts undergo a marked facilitation in CA1 but comparable studies are lacking for LPP–DG synapses. Results show profound differences between the two hippocampal synapses and suggest a novel type of filtering in the LPP. In all, specialized features of LPP–DG synapses lead to a marked transformation of afferent input from the entorhinal cortex and, as a result, the signal transfer to the pyramidal cell fields of hippocampus.

Methods

Ethical approval and animals

All studies used male C57/BL6 mice of 2−4 months of age. Animals were group-housed in cages of five with access to water and food *ad libitum* and maintained on a 12 h light–dark cycle. Electrophysiological experiments were initiated from 08.00 to 10.00 h. All procedures were in accordance with the Institutional Animal Care and Use Committee at the University of California, Irvine and the National Institutes of Health *Guidelines for the Care and Use of Laboratory Animals*. For all electrophysiology studies, mice were anaesthetized with isoflurane and euthanized by decapitation. Experiments complied with the animal ethics checklist and guidelines laid down by *The Journal of Physiology*.

Extracellular field recordings

Hippocampal slices were prepared from adult (3–4 months old) male C57/BL6 mice as previously described (Cox et al., 2019; Gunn et al., 2017). Briefly, brains were rapidly removed and placed in ice-cold, oxygenated (95% O_2–5% CO_2) high Mg^{2+} artificial cerebrospinal fluid (aCSF) containing (in mM): 87 NaCl, 26 $NaHCO_3$, 25 glucose, 75 sucrose, 2.5 KCl, 1.25 NaH_2PO_4, 0.5 $CaCl_2$, 7 $MgCl_2$ (320–335 mOsm). Horizontal sections (350–400 μm) were cut using a Leica Vibratome (model VT1000s, Leica, Deer Park, IL, USA) at 4°C. Slices were rapidly transferred to an interface recording chamber maintained

at 31 ± 1°C with constant perfusion (60–70 ml/h) of oxygenated (95% O_2–5% CO_2) aCSF containing (in mM): 124 NaCl, 3 KCl, 1.25 KH_2PO_4, 1.5 $MgSO_4$, 26 $NaHCO_3$, 2.5 $CaCl_2$, and 10 dextrose (300–310 mOsm, pH 7.4). Recordings began ~1.5–2 h later. A stimulating (twisted nichrome wire) electrode was placed within the outer third of the DG molecular layer (OML) targeting the LPP, and glass (2 M NaCl, 2−3 MΩ) recording electrodes were placed in the OML (dendritic responses) or within the granule cell layer (population spike responses) of the DG. Paired-pulse stimulation (40 ms interval) was used to confirm facilitation, as is characteristic of the LPP (Christie & Abraham, 1994; Wang et al., 2016). Stimulation strength was adjusted to elicit a field excitatory postsynaptic potential (fEPSP) that was 50% of the maximum population spike free response; responses to 0.05 Hz stimulation were recorded thereafter. For cell layer recordings, stimulation was adjusted to achieve population spike amplitudes of 1−2 mV with responses similarly evoked at a frequency of 0.05 Hz. The effect of repetitive stimulation was tested by delivering 10 pulse trains at 5 Hz (θ), 20 Hz (β) or 50 Hz (γ) after 10 min of stable baseline. Delivery of the different trains was randomized, with no difference in responses to order and each train was separated by a minimum of 10 min to prevent potentiation or depression in responses. A subset of experiments investigated the effect of stimulating the LPP–DG synapse with a physiologically relevant pattern of activity consisting of five high frequency bursts (50 Hz; three pulses) separated by 200 ms ($\theta\gamma$). The effect that the inter-burst interval had upon the burst response was tested by increasing the duration to 1 s and then to 5 s to establish a time course for the different forms of synaptic filtering that occurred.

In a number of experiments, responses were additionally recorded from the CA3–CA1 synapse. Field EPSPs were elicited from CA1b stratum radiatum as previously described (Le et al., 2022), and the effect of repetitive γ frequency stimulation and $\theta\gamma$ bursts assessed as described above.

Inhibition of medial perforant path–DG synapses.—A subset of experiments tested the specificity of our LPP stimulation protocol by pharmacologically inhibiting transmission at the medial perforant path (MPP)–DG synapse with the mGluR II/III agonist DCG IV (1 μM). A stimulating electrode and a glass recording electrode were placed in the middle third of the DG molecular layer, separated by ~500–600 μm, to record MPP-evoked dendritic fEPSPs. Paired-pulse suppression (40 ms interval) and the frequency-dependent depression of responses to brief stimulation trains (5, 20 and 50 Hz), characteristic of MPP synapses (Christie & Abraham, 1994; McNaughton, 1980, 1982), were used to confirm placement. Responses to 10 pulses stimulation trains delivered at θ, β or γ frequencies (separated by >10 min) were obtained prior to recording a stable baseline period of at least 20 min (0.05 Hz stimulation). DCG IV was then applied to the chamber via a second perfusion line (6 ml/h) for at least 40 min to confirm the inhibitory effect upon baseline responses. A second set of experiments investigated the effect of DCG IV upon LPP-evoked dendritic responses. Responses to brief stimulation trains (10 pulses; θ, β or γ frequencies at 10 min intervals) were obtained prior to recording a stable baseline period (0.05 Hz stimulation; 20 min). DCG IV was then infused (>40 min) to assess the effect upon baseline responses before repeating the stimulation trains (at 10 min intervals) in the presence of the agonist.

Treatment with selective antagonists.—A subset of experiments tested the effect that bath application of picrotoxin (PTX: 1 μM) or apamin (200 nM), to inhibit $GABA_A$R-mediated inhibition and SK channel function, respectively, had upon LPP-evoked baseline transmission and the responses to both repetitive (20 Hz and/or 50 Hz) and burst patterns ($\theta\gamma$) of stimulation. Responses to stimulation trains (either repetitive or bursts) were obtained prior to recording a stable baseline period of at least 20 min (0.05 Hz stimulation). Stimulation trains were separated by >10 min. PTX or apamin was then applied to the chamber via a second perfusion line for at least 40 min to assess the effect upon baseline responses before repeating the stimulation trains (at 10 min intervals) in the presence of the antagonist. As a positive control, the effects of apamin upon baseline responses and repetitive γ frequency (50 Hz) stimulation were tested in field CA1.

Low external Ca^{2+} experiments.—The effect that lowering the release probability (*P*) had upon the responses to repetitive LPP stimulation (i.e. 10 pulse trains at 5, 20 or 50 Hz) as well as to $\theta\gamma$ bursts was tested in a subset of experiments, where slices were perfused with a low Ca^{2+} aCSF (in mM: 124 NaCl, 3 KCl, 1.25 KH_2PO_4, 3 $MgSO_4$, 26 $NaHCO_3$, 1 $CaCl_2$ and 10 dextrose; 300–310 mOsm, pH 7.4) immediately following slice preparation.

LTP experiments.—In separate experiments we investigated how induction of long-term potentiation (LTP) at the LPP–DG synapse influenced synaptic filtering. Responses to stimulation trains delivered to the LPP at 5, 20 and 50 Hz (each separated by >10 min) were collected prior to recording a 20 min period of stable baseline responses. LPP-LTP was then induced using a single, 1 s train of 100 Hz high frequency stimulation (HFS) with pulse duration doubled and intensity increased by 1.5× relative to baseline stimulation. Stimulation trains (i.e. 5, 20 and 50 Hz) were repeated 60 min after HFS stimulation and the responses collected. As a control for temporal drift of the evoked responses, stimulation trains were delivered at each of the frequencies as described above with slices being left for 60 min (no LTP induction) before repeating the stimulation trains.

Responses to set-frequency stimulation trains were collected using NACGather 2.0 (Theta Burst Corp. Irvine, CA, USA) and then analysed offline using NACShow 2.0 (Theta Burst Corp. Irvine, CA, USA). Slopes (20–80%) of the leading edge of the fEPSPs were measured across the train and were normalized as the percentage ratio of the first pulse. For $\theta\gamma$ trains, the slope of each fEPSP was measured. The slope of fEPSPs was normalized (as the percentage ratio) to (1) the slope of the initial fEPSP in the first burst response (to test for overall facilitation across the burst train) and (2) the first response of their respective burst. This enabled a comparison of the overall facilitation across the burst train, as well as the magnitude of within-burst facilitation across successive bursts. For drug treatment studies (i.e. PTX, apamin), stable baseline responses, collected over a 20 min period, were analysed with regard to peak amplitude, rising slope and half-width of the fEPSP. The decay phase of a digitally averaged fEPSP (20 events) was described using a single exponential equation. The fEPSP slope in response to stimulation trains (repetitive or burst patterns) in the absence and presence of the specific agonist/antagonist was normalized as described above. The magnitude of LTP was determined by comparing the fEPSP slope of responses collected during the last 5 min of a 20 min, pre-HFS baseline period with those obtained during the

last 5 min of the recording (i.e. 55−60 min post-LTP induction). The paired pulse ratio (40 ms interval) was analysed before and 60 min after LTP induction.

Whole-cell recordings

Hippocampal slices for whole-cell electrophysiology were prepared as previously described (Wang, Jia et al., 2018). Briefly, the brain was rapidly removed and placed in ice-cold oxygenated (95% O_2–5% CO_2) aCSF containing (in mM): 124 NaCl, 3 KCl, 1.25 KH_2PO_4, 3 $MgSO_4$, 26 $NaHCO_3$ and 10 dextrose (300–310 mOsm, pH 7.4). Transverse sections (350 μm) were cut using a Leica Vibratome (model VT1000s, Deer Park, IL, USA) at 4°C. Slices were transferred to a holding chamber and incubated at room temperature in oxygenated (95% O_2–5% CO_2) aCSF containing (in mM): 124 NaCl, 3 KCl, 1.25 KH_2PO_4, 1.5 $MgSO_4$, 26 $NaHCO_3$, 2.5 $CaCl_2$ and 10 glucose (300–310 mOsm, pH 7.4). At least 1 h after preparation, slices were transferred to the recording chamber where they were continuously perfused in oxygenated aCSF (above).

A small diameter (1 μm) bipolar stimulating electrode (World Precision Instruments Inc., Sarasota, FL, USA), placed in the DG OML adjacent to the fissure and overlying the recorded granule cell, was used to evoke LPP-specific responses. Patch pipettes (5–8 MΩ) were pulled from thick-walled borosilicate glass (1.5 mm outer diameter; 0.86 mm inner diameter; Sutter Instrument Co., Novato, CA, USA) and filled with an internal solution containing (in mM): 130 $CsCH_3SO_4$, 8 CsCl, 8 NaCl, 10 Hepes, 0.2 EGTA, 2 Mg-ATP, 0.3 Na-GTP and 2 QX-314 (Sigma, St Louis, MO, USA). Under these conditions, the calculated (pClamp 10, Molecular Devices, San Jose, CA, USA) and experimentally verified reversal potentials for glutamate ($E_{glutamate}$) and GABA (E_{GABA}) were 0 and −55 mV, respectively. LPP evoked excitatory postsynaptic currents (eEPSCs) were recorded from DG granule cells (30 ± 1°C) at a holding potential of −70mV in aCSF that additionally contained the $GABA_AR$ antagonist PTX (50 μM). Paired pulse stimulation (40 ms interval) was used to confirm the characteristic facilitation at the LPP–DG synapse (Christie & Abraham, 1994; McNaughton, 1980, 1982). Stimulation trains (10 pulses) were delivered at θ, β and γ frequencies with a 3 min interval between trains. In a subset of experiments eEPSCs were recorded (30 ± 1°C) from granule cells at a holding potential of −50 mV in aCSF (above) that additionally contained the NMDAR and $GABA_AR$ antagonists 2-amino-5-phosphonopentanoic acid (AP-5, 50 μM) and bicuculline (20 μM), respectively. Responses to brief γ frequency bursts (three pulses; 50 Hz) separated by 200 ms (five bursts; $\theta\gamma$) were recorded either with or without the Ca^{2+} chelator BAPTA (10 mM) in the internal solution (above). Finally, LPP eIPSCs were recorded from DG granule cells (30 ± 1°C) at a holding potential of 0 mV in the absence of glutamate receptor antagonists. Stimulation trains (10 pulses) were delivered at 5, 20 and 50 Hz with each train separated by 3 min. Currents were filtered at 2 Hz using an 8-pole Bessel filter. Only those cells with a stable access resistance were used, and recordings were aborted if >20% change in series resistance occurred. Recordings for both sets of experiments were performed using an Axopatch 200A (Molecular Devices, San Jose, CA, USA) and pClamp 10 and stored directly to a PC (4 kHz digitization) using a Digidata 1550A (Molecular Devices, San Jose, CA, USA).

All recordings were analysed offline using the Strathclyde Electrophysiological Software (WinEDR and WinWCP; Dr J Dempster, University of Strathclyde, UK). Ensemble averages (three events) of a single eIPSC generated for each cell were analysed with regard to peak amplitude and decay time course. The decay phase was best described by the single exponential function $Y(t) = A e^{-1/\tau}$. The peak amplitude of eEPSCs and eIPSCs was measured across the train and then normalized as the percentage ratio of the first pulse. The decay phase of the final inhibitory response of each stimulation train was described using the above single exponential function. For $\theta\gamma$ stimulation, the eEPSCs (in the presence or absence of BAPTA) were analysed with regard to peak amplitude and responses were then normalized (as the percentage ratio) to (1) the initial eEPSC in the first burst response (to test for overall changes across the burst train) and (2) the first response of their respective burst. This enabled a comparison of the overall facilitation across the burst train and the magnitude of within burst facilitation across successive bursts.

Drug application

Drugs were made fresh on day of use. For field recording studies, the $GABA_AR$ antagonist PTX was prepared as a stock solution (10 mM) in dimethyl sulfoxide (DMSO), whereas the SK channel antagonist, apamin (250 μM), and the mGluR II/III agonist, DCG IV (10 mM) were made as stock solutions in distilled water (all from Tocris Biosciences, Minneapolis, MN, USA). Each was then diluted in aCSF to attain the desired final concentration, for PTX containing a final DMSO concentration at <0.1% (PTX, 1 μM; apamin 200 nM; DCG IV, 1 μM). For whole cell recordings, the NMDAR antagonist AP-5 (HelloBio, Princeton, NJ, USA) and the $GABA_AR$ antagonist bicuculline (Tocris Biosciences, Minneapolis, MN, USA) were made as stock solutions in distilled water and diluted to the final concentration in aCSF (50 mM and 20 mM, respectively). PTX was made as a stock solution (50 mM) in DMSO. The Ca^{2+} chelator, BAPTA (Tocris Biosciences, Minneapolis, MN, USA) was made directly in the internal solution to a concentration of 10 mM.

Immunofluorescence

For analysis of VGLUT synaptic localization, adult mice ($n = 5$) were anaesthetized with isoflurane and euthanized by decapitation. Brains were removed and quick-frozen in −40°C 2-methylbutane and then cryostat-sectioned at a thickness of 25 μm on the coronal plane through hippocampus and thaw-mounted onto Superfrost Slides (Thermo Fisher Scientific, Waltham, MA, USA). After fixation in 4% paraformaldehyde in 0.1 M phosphate buffer pH 7.2 (PB) the tissue was processed for dual immunofluorescence as described (Rex et al., 2009; Seese et al., 2013, 2014) using knockout-verified antisera from Synaptic Systems GmbH (Göttingen, Germany) including polyclonal guinea pig anti-VGLUT1 (Synaptic Systems no. 135304; RRID AB_887878) or anti-VGLUT2 (Synaptic Systems no. 135404; RRID AB_887884) in combination with rabbit anti-Synaptotagmin-7 (Synaptic System no. 105137; RRID AB_887838) all at 1:1000 dilution in PB containing 0.3% Triton X-100 and 3% normal swine serum. Secondary antisera included AlexaFluor 488 goat anti-guinea pig IgG and AlexaFluor 594 goat anti-rabbit IgG (1:1000; Thermo Fisher Scientific, Waltham, MA, USA). Tissue was coverslipped with Vectashield containing 4′,6-diamidino-2-phenylindole (DAPI; Vector Laboratories, Burlingame, CA, USA).

Entorhinal cortex lesion

For verification of VGLUT localization in the perforant path, an additional three mice received unilateral electrolytic lesion of the entorhinal cortex as previously described (Guthrie et al., 1995; Lynch et al., 1972); the contralateral unlesioned side served as control. Mice were anaesthetized with a ketamine–xylazine cocktail (100 mg and 10 mg/kg intraperitoneal), and an electrode (insulated stainless steel wire) was lowered into the lateral entorhinal cortex (from lambda; anterior–posterior: +1.0, medial–lateral: −4.0, dorsal–ventral: −4.8), unilaterally. A current was passed through the electrode at 0.8 mA for 20 s. After surgery, mice were returned to their home cage for recovery. These mice were euthanized 4 days post-lesion with an overdose of euthasol and intracardially perfused with 4% paraformaldehyde in 0.1 M PB. After cryoprotection, brains were sectioned at a thickness of 35 μm on the horizontal plane through hippocampus, and the free-floating tissue sections were processed for localization of VGLUT1 or VGLUT2 (as above) and then slide-mounted and coverslipped with Vectashield containing DAPI.

Analysis of synaptic localization /fluorescence deconvolution tomography

For analysis of synaptic localization, image z-stacks were collected from field CA1b stratum radiatum and the OML and middle molecular layer (MML) that contains the lateral (LPP) and medial perforant path (MPP) innervation, respectively, using a Leica DM6000B epifluorescence microscope equipped with a Ludl stage with a BioPrecision Stepper motor driven by Volocity 4.0 software (PerkinElmer, Waltham, MA, USA). Images were collected at ×63 (1.4 NA) at 0.2 μm intervals through a depth of 3 μm for a 135 × 105 × 3 μm (42,525 μm^3) sample field in CA1. For the LPP and MPP fields, two adjacent image stacks (with ~10% overlap) were collected from the internal blade of the DG molecular layer; the long edge of the first image field was adjacent to and aligned with the hippocampal fissure and the second was placed immediately proximal to this. The DAPI counterstain was used to align and digitally stitch the z-stack into one continuous image using pairwise stitching in Fiji and the larger image stack was then segmented to quantify the synaptic labelling in the outer and middle molecular layers containing LPP and MPP innervation, respectively (Wang, Cox et al., 2018). Images were collected from both CA1 and DG fields for five tissue sections per brain. Quantitative fluorescence deconvolution tomography (FDT) analysis entailed processing images through restorative deconvolution (99% confidence; Volocity 4.0, PerkinElmer) and used to construct a 3-dimensional (3D) montage of the sample field. Within that montage, immunolabelled objects were detected using threshold segmentation separately for each channel: the image was normalized for background density and objects were segmented based on connected pixels above threshold using in-house software that employed C, Java, MATLAB (The MathWorks Inc., Natick, MA, USA) and Perl (Granger et al., 1989; Lauterborn et al., 2021; Rex et al., 2009). Immunofluorescent elements meeting the size and eccentricity constraints of synapses, and detected across multiple intensity thresholds, were quantified using automated systems (Rex et al., 2009; Wang, Jia et al., 2018; Wang, Le et al., 2018). Elements were considered double-labelled if there was contact or overlap of fields occupied by the two fluorophores as assessed in 3D. For each z-stack these procedures identified approximately 30,000 reconstructed terminal synapses for field CA1 and 15,000 terminal synapses in each of the LPP and MPP fields. Thus, metrics were collected from approximately 150,000 and 75,000 synapses for CA1 and perforant path

fields, respectively, for each animal. With this approach we have successfully identified localization to pre- and post-synaptic compartments in multiple studies (Chen et al., 2010; Wang, Le et al., 2018).

Monte Carlo simulations of a two-step release model

We implemented a previously published (Miki et al., 2016) renewable two-step synaptic release model based upon Monte Carlo simulations using Igor Pro (Wavemetrics, Lake Oswego, OR, USA) to test if the operation of factors within the presynaptic terminal could account for the LPP–DG filter. The two-step model incorporates four factors associated with the release and subsequent recycling of synaptic vesicles. These include the probability of docking site occupancy (δ) and the probability of docked vesicle release (p_v). The overall probability of release (p) is described by the product of these two factors ($p = \delta p_v$). Each synapse has a number of docking sites (N) that are associated with a pool of replacement vesicles. The transition of a replacement vesicle to an empty docking site is described by the probability 'r.' Before stimulations the occupancy probability of the replacement pool is fixed at 1, with replenishment of the replacement pool occurring with a probability 's' following depletion of the replacement vesicle(s).

A parameter search was conducted to identify the combination of variables that most accurately recapitulated the experimental data recorded from LPP–DG, MPP–DG and CA3–CA1 synapses following stimulation at 50 Hz (10 pulses). Simulations were run using the version of the model by Miki et al. with the common replacement pool. The code was slightly modified to compute a parameter space across variables δ, p_v, r, s, docking site number, and replacement pool size with the following constraints: $\delta p_v < 0.3$ for low-p synapses; $\delta p_v < 0.6$ for high-p synapses; $r > 0.2$ and < 0.8; s > 0.2 and < 0.8; docking site number ≥ 3 and ≤ 8; replacement pool size ≤ 20 (replacement pool size $\geq$ docking site number). The simulation was repeated 50 times for each combination of variables. The simulated output, mean vesicle number, was normalized to the initial response (i.e. pulse 1) and then fit to the normalized curves generated experimentally. The standard error between each individual point (i.e. pulse number) was compared and a mean value generated. The parameter search was conducted using custom code generated using Python 3.8.

Combining high and low probability of release synapses.—Using the parameters found to most reliably recapitulate the MPP–DG and CA3–CA1 curves (putative high- and low-p synapses, respectively) we tested if a weighted combination of the two synapses could reproduce the experimentally measured LPP–DG responses. Using a custom written code (Python 3.8), the optimum ratio of the two curves was established. In order to generate the best fit between the simulated and experimentally derived data, a scale factor was required. The combined output of the two curves was generated using the following equation:

$$\text{LPP} - \text{DG} \approx x(\text{CA3} - \text{CA1}) + y(\text{MPP} - \text{DG})$$

The above equation was additionally used to generate a combined curve of the electrophysiological CA3–CA1 and MPP–DG responses.

Investigating the effect of replacement pool size.—Using the optimal parameters for the low- (i.e. CA3–CA1) and high- (MPP–DG) p synapses the effect of changing the number of replacement vesicles influences the simulated output was tested.

Reducing p at the simulated LPP–DG synapse.—Using the single set of parameters that best described the experimentally derived LPP–DG responses, p was reduced by incrementally lowering δ and p_v values. The output was then fit to the experimentally derived LPP–DG responses recorded under conditions of reduced external Ca^{2+}. The quality of fit was assessed by generating a mean standard deviation for each point.

Statistical analysis

All results are presented as group mean values ± SD. Statistical comparisons of the properties of fEPSPs before and after drug treatment were made using paired two-tailed Student's t-test. Two-way repeated measures (RM)-ANOVA (GraphPad Prism version 6.0, GraphPad Software Inc., San Diego, CA, USA) was used to determine the statistical significance of drug treatment, LTP and reduced external Ca^{2+} upon normalized responses to repetitive and $\theta\gamma$ patterns of LPP stimulation. For electrophysiological studies, the group n refers to the number of slices (extracellular recordings) or cells (whole-cell recordings) studied, from a minimum of three animals. For analyses of immunofluorescence frequency distribution curves, RM-ANOVA was used (GraphPad Prism version 9.1.1). Paired Student's t-test or one-way ANOVA followed by Tukey's multiple comparison test was used for comparisons of high density labelled synapses between two or three fields, respectively. Each group consisted of five animals. For all studies, P-values <0.05 were considered significant.

Results

The lateral perforant path operates as a low-pass filter

To assess the functional characteristics of LPP synapses, 10-pulse trains were delivered to the LPP at three frequencies – θ (5 Hz), β (20 Hz) and γ (50 Hz) – known to occur in the entorhinal cortex and hippocampus during processing of spatial cues (Colgin, 2016). With 5 Hz stimulation, fEPSP slopes recorded from the LPP–DG exhibited a modest initial facilitation that gradually decreased in magnitude over the course of the train with the last pulse producing a near baseline response (pulse 10: 97 ± 12.54%; n = 21 slices/9 mice). β frequency stimulation produced a larger initial facilitation followed by a rapid decrease in response size over successive pulses (pulse 10: 93 ± 15.27%; n = 22 slices/9 mice). In accord with earlier reports (Wang, Jia et al., 2018), γ trains produced a striking within-train reduction in fEPSP slope beginning with the fourth pulse (pulse 10: 57 ± 14.68%; n = 22 slices/9 mice; Fig. 1*A* and *B*). The β and γ stimulation results for the LPP are dramatically different from those described for the CA3–CA1 link in hippocampal circuitry (Amani et al., 2021; Koutsoumpa & Papatheodoropoulos, 2019; Trieu et al., 2015). We confirmed that the latter connections exhibit robust facilitation throughout a 50 Hz train (pulse 10: 127 ± 17.15%; n = 8 slices/5 mice) (Fig. 1*B*).

In a separate set of experiments, we addressed the question of how the output of the LPP target neurons (i.e. granule cell spiking) was influenced by the LPP–DG filter. Stimulation currents were increased to a level sufficient to produce a small population spike (1–2 mV amplitude) after which θ, β, and γ trains were applied in an ascending or descending order. Results paralleled those for the dendritic fEPSPs, but were more pronounced. In response to a 5 Hz train, the population spike amplitude was amplified dramatically from the first to the second pulse and was then maintained across the duration of the train with responses by the 10th pulse being significantly greater than baseline (pulse 10: 256 ± 132.83%; n = 7 slices/4 mice). In contrast, responses to LPP stimulation at β frequency were initially facilitated (pulse 2: 293 ± 88.82%; n = 7 slices/4 mice), but successive pulses elicited progressively smaller population spikes such that the response fell to the original response by pulse no. 10 (pulse 10: 94 ± 70.64%; n = 9 slices/4 mice). Stimulation at γ frequency again produced dramatic results: population spikes were undetectable from the third or fourth pulse forward (Fig. 1*C* and *D*).

The co-activation of MPP fibres located in the middle third of the molecular layer (Hjorth-Simonsen, 1972; Steward, 1976; Witter, 1993) could, given the previously reported frequency-dependent suppression of responses (McNaughton, 1980, 1982), contribute to the filtering operations described at the LPP–DG synapse. To explore this notion, we tested the LPP–DG filter in the presence of DCG IV (1 μM), an mGluR II/III agonist that inhibits transmission at the MPP–DG synapse (Bough et al., 2004; Macek et al., 1996; Rohde et al., 2012). Initial experiments confirmed that (1) MPP-evoked responses exhibited the previously described frequency-dependent suppression following brief stimulation trains (Fig. 2*A*) and (2) DCG IV inhibited MPP–DG transmission (Fig. 2*B* and *C*). Having confirmed that DCG IV significantly attenuated MPP-evoked responses, we next tested the effect that bath application of DCG IV had upon LPP-evoked dendritic responses. The agonist produced a modest yet significant decrease in the baseline fEPSP (Fig. 2*B–D*), while no effects upon responses to brief stimulation trains in the β range and above were observed (θ: $F_{(9,54)}$ = 2.075; P = 0.048; β: $F_{(9,54)}$ = 1.533; P = 0.1601; γ: $F_{(9,54)}$ = 1.057; P = 0.4088; n = 7 slices/4 mice; two-way RM-ANOVA; Fig. 2*E* and *F*). Whether the DCG IV-induced decrease in the baseline response and increased facilitation following LPP stimulation at θ frequencies is a result of reduced stochastic release from MPP terminals or the direct stimulation of this pathway remains to be determined. Collectively, these findings indicate that the LPP filter is not due to partial activation of MPP inputs.

In all, the LPP–DG synapses act as low pass filters for inputs from the lateral entorhinal cortex: they follow 5 Hz and 20 Hz inputs but quickly depress during 50 Hz γ stimulation. The latter depression does not appear to involve significant recruitment of MPP inputs. The next stage of processing – evoked spiking by the target neurons – exaggerates the signal transformation occurring in the dendrites.

Recruitment of GABAergic transmission is not critical for the LPP–DG low pass filter

Feedforward GABAergic interneurons produce a strong shunting effect on AMPAR-mediated currents following activation of the CA3 inputs to field CA1 (Arai et al., 1995; Davies et al., 1991; Larson & Lynch, 1986; Larson & Munkacsy, 2015; Mott & Lewis,

1991; Pacelli et al., 1989). We tested for this version of postsynaptic filtering in the LPP–DG connections using bath application of the $GABA_AR$ antagonist PTX (1 μM). The compound had no significant effect on the amplitude or initial slope of fEPSPs but did produce a significant increase in the waveform half-width and decay time (half-width, $P = 0.007$; τ, $P = 0.012$; paired Student's t-test; Fig. 3*A* and *B*). Within-train suppression of responses produced by activation of LPP inputs in the β range (20 Hz) showed a modest yet significant reduction with PTX present (baseline pulse no. 10: 73 ± 8.37%, PTX pulse no. 10: 88 ± 9.50%; $n = 5$ slices/2 mice; $F_{(9,36)} = 2.17$, $P = 0.049$; two-way RM-ANOVA; Fig. 3*C* and *D*), but no significant effect of PTX was observed with γ frequency activation (baseline pulse 10: 48 ± 2.70%, PTX pulse 10: 57 ± 7.29%; $n = 5$ slices/2 mice; $F_{(9,36)} = 1.13$, $P = 0.378$; two-way repeated measures ANOVA. Fig. 3*E* and *F*). These findings suggest that repetitive stimulation results in only a modest, frequency-dependent increase in the level of $GABA_AR$-mediated inhibition on granule cells. We further explored this idea using whole-cell voltage-clamp recordings of LPP-eEPSCs from DG granule cells with GABAergic transmission completely blocked (50 μM PTX). Under these conditions, a similar frequency-dependent suppression of the eEPSC amplitude was evident (Fig. 3*G* and *H*). These data further support the conclusion that the low-pass filter at the LPP–DG synapse is not critically dependent upon the recruitment of feedforward GABAergic inhibition.

Although GABAergic inhibition does not appear to be heavily involved in the low pass filter at the LPP–DG synapse, the recruitment of feedforward interneurons that innervate other somato-dendritic sites may be important in modulating the DG spike output (i.e. local circuit activation). To explore this further we tested the effect of bath applied PTX (1 μM) upon the granule cell output (i.e. 1−2 mV population spike). Bath application of the $GABA_AR$ antagonist produced a significant increase in the baseline population spike amplitude of single responses (baseline: 1.0 ± 0.58 mV; PTX: 3.4 ± 2.35 mV; $t_5 = 3.10$, $P = 0.027$; $n = 6$ slices/4 mice; paired Student's t-test; Fig. 4*A* and *B*). The amplification of the population spike observed following LPP activation in the θ range was not significantly influenced by PTX ($F_{(9,54)} = 0.9938$, $P = 0.4562$; $n = 7$ slices/4 mice; two way RM-ANOVA; Fig. 4*C*). The within-train suppression of the population spike amplitude observed with β frequency stimulation was significantly increased on the second pulse whilst γ frequency LPP activation was unaffected by PTX (β: $F_{(9,45)} = 3.932$, $P = 0.001$; γ: $F_{(9,45)} = 0.0231$, $P > 0.999$; $n = 6$–7 slices/4 mice; Fig. 4*D* and *E*). These data indicate that recruitment of GABAergic interneurons does not contribute significantly to the modulation of granule cell output following brief LPP activation at θ, β and γ frequencies.

We further investigated the effects of $GABA_AR$-mediated inhibition using the whole-cell voltage clamp configuration to record LPP-eIPSCs and examined how these responses were influenced during repetitive stimulation in the θ, β and γ ranges. With the membrane voltage held at 0 mV, which is the AMPAR reversal potential (E_{AMPA}), application of bicuculline (20 μM) produced a complete suppression of the evoked response (Fig. 4*F*). LPP-evoked IPSCs had a large peak amplitude (192 ± 54.23 pA; $n = 11$ cells/4 mice) and relatively slow decay time course ($\tau = 90 \pm 25.64$ ms; $n = 11$cells/4 mice; Fig. 4*G*). Consistent with previous studies (Ewell & Jones, 2010), there was a marked, frequency-dependent within-train suppression of eIPSCs (Fig. 4*H*–*K*). At higher stimulation frequencies, the decline in eIPSC amplitude was offset by prolongation of the decay time (Fig. 4*I*–*K*). Such

an effect may be indicative of 'spill over' activation of perisynaptic δ-$GABA_A$Rs, a receptor isoform highly expressed in granule cells (Wei et al., 2003) that is characterized by slow rates of desensitization and is typically associated with mediating a tonic form of inhibition (Nusser et al., 1998; Saxena & Macdonald, 1994; but see Sun et al. (2020) for contribution to phasic transmission). These results likely reflect a failure of interneurons to follow higher frequency input as well as the saturation of a population of slowly desensitizing receptor isoforms.

Collectively, these data suggest that the LPP–DG low pass filter observed at the levels of the synapse and the granule cell output (i.e. population spike) does not involve the significant recruitment of feed-forward GABAergic transmission. The observation that LPP-eIPSCs show a pronounced frequency-dependent within-train suppression indicates an inability of DG interneurons to follow high frequency LPP activation, a feature that likely underlies the circuit level phenomena.

Decreasing external Ca^{2+} reduces low pass filtering at the LPP–DG synapse

The inability of LPP synapses to follow high rates of input, as described above, could involve a depletion of a readily releasable pool (RRP) of vesicles due to an initially high p or to a reduction in quantal size because of relatively slow neurotransmitter cycling (Edwards, 2007; Thomson, 2000). Reduced extracellular Ca^{2+} is commonly used to lower p, and we accordingly tested its effect on LPP frequency facilitation. There was a clear enhancement of frequency facilitation produced by θ trains in slices maintained in 1 mM Ca^{2+} (Fig. 5*A*; pulse 10: control: 98 ± 8.80%, low Ca^{2+}: 128 ± 21.72%; n = 7–12 slices/4−5 mice/group; $F_{(9,144)}$ = 9.365, P < 0.0001; two way RM-ANOVA) and yet greater enhancement with β (20 Hz) stimulation (Fig. 5*B*; pulse 10: control: 91 ± 7.34%, low Ca^{2+}: 173 ± 34.73%; n = 7–12 slices/4−5 mice/group; $F_{(9,144)}$ = 35.11, P < 0.0001; two way RM-ANOVA). Within-train facilitation was also markedly increased during γ stimulation in the presence of low external Ca^{2+} and the pronounced depression of responses evident with control medium (i.e. 2.5 mM Ca^{2+}) was largely eliminated (Fig. 5*C* pulse 10: control: 54 ± 11.91%, low Ca^{2+}: 148 ± 30.33%; n = 7–12 slices/4−5 mice/group; $F_{(9,153)}$ = 38.02, P < 0.0001; two way RM-ANOVA).

Although a principal effect of lowering the external Ca^{2+} concentration will be to modulate the initial p, additional Ca^{2+}-dependent processes within the post-synaptic site may potentially contribute to the observed synaptic filtering. In particular, activation of small conductance Ca^{2+}-dependent K^+ (SK) channels, located in the spine head, have been implicated in shunting fEPSPs recorded from CA1 pyramidal cells (Ngo-Anh et al., 2005; Wang et al., 2014). The expression of SK channels in the DG molecular layer (Sailer et al., 2004) raises the possibility that they may also shape responses to LPP stimulation. Bath application of the selective SK channel blocker apamin (200 nM) had no effect upon amplitude, slope or decay time of single LPP-evoked fEPSPs (Fig. 6*A*–*D*). However, a modest yet significant reduction in the within-train suppression of responses during γ (50 Hz) activation was observed (baseline pulse no. 10: 52 ± 9.62%, apamin pulse no. 10: 63 ± 19.47%, n = 8 slices/4 mice; $F_{(9,63)}$ = 2.290, P = 0.027; two-way RM-ANOVA; Fig. 6*E* and *F*). As a positive control, the effects of apamin were tested at the CA3–CA1

synapse. Bath application of apamin had no significant effect upon the amplitude, slope or half-width of baseline responses (amplitude $P = 0.387$; slope $P = 0.639$; half-width $P = 0.427$; paired Student's t-test), although the within-train facilitation of responses during γ frequency stimulation was significantly enhanced (baseline pulse no. 10: 120 ± 18.40%, apamin pulse no. 10: 146 ± 22.40%; $n = 7$ slices/5 mice; $F_{(9,54)} = 4.67$, $P = 0.0001$; two-way RM-ANOVA; Fig. 6*G* and *H*). These findings suggest that repetitive activation of LPP inputs is sufficient to drive the necessary increase in local Ca^{2+} to rapidly activate SK channels (Stocker, 2004) but that this effect is only minimally involved in filtering.

LTP modifies presynaptic filtering in the LPP

At the LPP–DG synapse, LTP is dependent upon presynaptic modifications that result in a reduction in paired pulse facilitation (PPF) (Wang et al., 2016) indicative of an increase in initial p. Based upon the findings described immediately above, this would be predicted to enhance within-train suppression of responses. We accordingly tested for interactions between the stable changes underlying LTP expression and the transient adjustments responsible for frequency facilitation.

Ten-pulse trains were administered to the LPP in a single slice at θ, β and γ frequencies; this was repeated 45–60 min later with the three trains delivered in the same order (high to low or low to high frequency) as followed in the first session. LTP was induced in some cases immediately after session 1 (Fig. 7*A* and *B*). A reduction in the PPF was observed following the induction of stable LTP, indicating an increased p (PPF pre-LTP: 43 ± 8.49%, PPF post-LTP: 28 ± 7.75%; $n = 5$ slices/3 mice; $P = 0.039$; paired Student's t-test; Fig. 7*C*). Analysis of the effects of LTP was complicated by a tendency towards an upward shift in frequency curves between sessions 1 and 2 in the control (no LTP) slices. The reasons for the between-session shifts in frequency facilitation curves are unclear. Whether the session effect reflects a modest adjustment in terminals elicited by 30 stimulation pulses or instead is due to an over time (up to 60 min) generalized change in the slice preparation is an interesting question for future work.

Because of the above observations, we assessed the effects of LTP on frequency facilitation by comparing responses to θ, β and γ stimulation for sessions 1 and 2 (Fig. 7*D* and *E*), in control slices and in those in which stable potentiation had been induced. No differences between groups were found during session 1 (5 Hz: $F_{(9,135)} = 1.85$, $P = 0.065$; 20 Hz: $F_{(9,153)} = 0.75$, $P = 0.704$; 50 Hz: $F_{(9,135)} = 1.56$, $P = 0.135$; $n = 11$ slices/7 mice; two way RM-ANOVA; Fig. 7*D*). During session 2, however, there were striking differences between the facilitation curves in the LTP *vs.* control groups. At each stimulation frequency, LTP both blunted the initial (pulse no. 2) facilitation and depressed responses to subsequent pulses, resulting in a significant downward shift in the curve relative to that observed for the second session in control slices. Thus, the earlier described modest and sustained increase in fEPSPs obtained with θ activation was reduced to near baseline levels in potentiated LPP synapses (interaction between pulse number and groups: $F_{(9,162)} = 5.41$, $P < 0.0001$; $n = 11$ slices/7 mice). The statistically significant separation between the control and LTP curves was maintained across the full extent of the β (interaction $F_{(9,153)} = 5.78$, $P < 0.0001$) and γ ($F_{(9,135)} = 5.85$, $P < 0.0001$) stimulation trains (Fig. 7*E*), suggesting that the factor(s)

responsible for the initial decrement in facilitation continue to operate across successive, repetitive inputs. In all, LTP markedly augments the strength of LPP synapses while also exaggerating frequency filtering of responses to higher frequency inputs.

Relative concentrations of synaptotagmin-7 and VGLUTs in LPP terminals

Vesicular glutamate transporters (VGLUTs) are essential for vesicle recycling, with evidence suggesting that VGLUT2 kinetics are slower than those for VGLUT1 (Nakakubo et al., 2020). Broadly speaking, VGLUT1 is found throughout the cortical telencephalon including all subfields of hippocampus and is associated with low-p synapses, while VGLUT2 predominates in subcortical structures that have synapses with a high p (Fremeau et al., 2001; Fujiyama et al., 2001). As such these transporters may provide a qualitative marker for the release properties of a given synapse.

Both VGLUT2 and VGLUT1 have been localized to the outer two-thirds of the DG molecular layer (Bellocchio et al., 1998; Kaneko et al., 2002), the terminal zone for the LPP and MPP projections that account for ~90% of all synapses in this field (Dolorfo & Amaral, 1998; Steward, 1976; Witter, 1993). We confirmed this observation using immunofluorescence. VGLUT2 immunoreactivity (-ir) was concentrated in the supragranular region and outer two-thirds of the DG molecular layer; modest VGLUT2-ir was evident in stratum lacunosum-moleculare of the hippocampus proper whereas other regions including the stratum radiatum field of CA3–CA1 termination had very low immunoreactivity. In contrast, VGLUT1-ir was more evenly distributed across fields (Fig. 8*A*), consistent with previous descriptions (Herzog et al., 2004). Next, we used fluorescence deconvolution tomography (FDT) to quantify levels of synaptic VGLUT immunoreactivity associated with the presynaptic marker synaptotagmin 7 (Syt7; Fig. 8*B*) and thereby test if the disparity in frequency facilitation curves for LPP–DG *vs.* CA3–CA1 synapses is associated with marked differences in the relative presynaptic concentrations of VGLUT1 and VGLUT2. FDT performs 3D reconstructions of image z-stacks and supports quantification of tens of thousands of single- and double-immunolabelled elements within the size constraints of synapses per image field. Results can be summarized as immunolabelling intensity frequency distributions which plot target protein immunolabelling densities in ascending bins on the x-axis and percentage double-labelled elements (target co-localized with the presynaptic marker Syt7) on the y-axis. The regional differences in VGLUT2 were dramatic: the intensity frequency curve for VGLUT2 in the DG OML (LPP field) was strikingly right shifted towards denser concentrations relative to that for terminals in CA1 stratum radiatum (sr) ($F_{(50,400)} = 63.52$; $P < 0.0001$; Fig. 8*C*). As expected, the percentage of terminals with high levels of the VGLUT2-ir (>100 on the intensity scale) was 2-fold higher in the OML *vs.* CA1 ($P = 0.0001$, Tukey's test; Fig. 8*D*); the percentage of terminals with very high levels of VGLUT2 was comparable between the outer and middle molecular layer fields of LPP and MPP termination respectively ($P = 0.558$, Tukey's test).

VGLUT1 has been localized to both DG and CA1 dendritic fields in multiple studies (Bellocchio et al., 1998; Fremeau et al., 2001; Halasy et al., 2004). Quantitative comparisons of the FDT intensity frequency distributions revealed a slight but significant difference in per terminal VGLUT1-ir between these fields ($F_{(31\ 248)} = 5.533$; $P < 0.0001$; Fig. 8*E*) but

the proportion of terminals with very high levels of VGLUT1 did not differ ($P = 0.3781$, Tukey's test; Fig. 8*F*). It thus appears that the balance of the two vesicle transporters in the LPP is markedly shifted in favour of VGLUT2.

As noted, residual Ca^{2+} is a key factor in frequency facilitation and computational studies concur with this conclusion. Recent work indicates that the Ca^{2+} sensor protein, Syt7 mediates the effects of residual Ca^{2+} on facilitation (Jackman et al., 2016) and it was accordingly of interest to compare concentrations of this presynaptic protein in DG OML and CA1 sr fields. The density frequency distributions for Syt7-ir in bouton-sized profiles were similar between the OML and CA1 sr ($F_{(50,400)} = 1.358$, $P = 0.0602$; Fig. 8*G*), as were the high density Syt7-ir terminals in each field ($P = 0.8859$; paired Student's *t*-test; Fig. 8*H*). These results indicate that differences in Syt7 levels do not account for differences in frequency facilitation between LPP and CA3–CA1 synapses and verify that Syt7 is an unbiased presynaptic marker for the VGLUT analysis described above.

Finally, to verify that clusters of VGLUT2-ir, in the DG OML, are indeed localized to perforant path terminals (Halasy et al., 2004) we evaluated effects of unilateral electrolytic lesion of the entorhinal cortex. As this projection is virtually unilateral in mid- to temporal hippocampus the contralateral side served as the control for evaluating effects of deafferentation. As assessed 4 days after entorhinal cortex lesion placement, there was near complete elimination of VGLUT1-ir and VGLUT2-ir within the distal DG molecular layer and stratum lacunosum-moleculare ipsilateral to the lesion, relative to robust labelling in these fields on the contralateral side (Fig. 8*I*); this is consistent with localization in the perforant path and temporo-ammonic systems, respectively.

Presynaptic factors may contribute to the low pass filter at the LPP–DG synapse

The findings from our electrophysiological studies indicate that the low pass filter at the LPP–DG synapse appears to be dependent upon factors within the presynaptic terminal. Given the difficulty in investigating mechanisms that underlie release dynamics empirically, we ran Monte Carlo simulations of a two-step synaptic release model (Miki et al., 2016) to test if presynaptic factors alone could recapitulate the LPP–DG filter. The two-step model incorporates factors associated with the release including the probability of vesicle docking (δ) and the release probability of a docked vesicle (p_v), as well as the probability of vesicles transitioning from the replacement pool to vacant docking sites (r) and replenishment of the replacement pool (s; Fig. 9*A* and Methods).

Initially, we tested if Monte Carlo simulations of this two-step model were capable of recapitulating the LPP–DG low pass filter in response to γ frequency stimulation. Using a model with three docking sites, replacement pool size of three vesicles and optimized release and replenishment parameters ($\delta = 0.6$, $p_v = 0.55$, $r = 0.7$ and $s = 0.4$), we were able to generate an output curve remarkably similar to our electrophysiological data (mean SD = 0.047; Fig. 9*B*). However, evidence that the relative expression of VGLUT1 and VGLUT2 in the dentate gyrus LPP field differs from that at the CA3–CA1 synapse (Fig. 8) raises the suggestion that the LPP–DG filter could be produced by a different combination of high- and low-p synapses. To explore this notion further we first tested if simulated low- (i.e. VGLUT1) and high- (i.e. VGLUT2) p synapses were capable of

generating output profiles that resembled those recorded electrophysiologically from CA3–CA1 and MPP–DG synapses – putative low- and high-p synapses. When constrained by the overall p (i.e. $p_V\delta$, see Methods) and with all other variables optimized, the two-step model was capable of reliably generating the facilitation and suppression of simulated responses typically associated with low- (i.e. CA3–CA1; Fig. 9*C*, SD = 0.019) and high-(i.e. MPP–DG; Fig. 9*D*, SD = 0.066) p synapses. Having established that the simulation could reliably reproduce the output curve associated with low- and high-p synapses following γ frequency stimulation, we next investigated how changes in the replacement pool size could influence the nature of this curve. At the low-p synapse, reducing the pool size caused a pronounced suppression of the within-train facilitation (Fig. 9*C*), while increasing the pool size delayed the overt depression of release at a putative high-p synapse (Fig. 9*D*). This indicates that the size of the replacement pool is a critical determinant of the output curve generated at both high- and low-p synapses. Next, we explored if the LPP–DG low pass filter could be generated by a mixed population of lowand high-p synapses. A parameter search revealed that combining the simulated CA3–CA1, where the pool size was reduced from five to three vesicles, and the MPP–DG curves was capable of reproducing the LPP–DG curve recorded experimentally when fit with a scale factor (Fig. 9*E*, SD = 0.123). The application of the scale factor indicates that an approximately 4:1 ratio of CA3–CA1 type to MPP–DG type synapses is required to recapitulate the experimentally measured LPP output curve. We next tested whether it was possible to combine the electrophysiologically recorded CA3–CA1 and MPP–DG output curves in a similar manner (i.e. scaled) to reproduce the LPP-evoked responses. Using the same approach, we found that the empirically measured responses could be combined to recapitulate the LPP–DG curve, albeit with a different scale factor (Fig. 9*E*, SD = 0.082). This latter point likely reflects difference between responses generated using a simulated single synapse and the factors occurring across a population of neurons that are responsible for producing the local field potential responses.

Our experimental data indicate that reducing p by lowering the external Ca^{2+} concentration largely attenuated the low pass filter observed at the LPP–DG synapse following γ frequency stimulation. As such we next tested if reducing p in the simulated LPP–DG synapse reproduced the electrophysiological data. Under conditions where only the initial p (i.e. δp_V) was reduced, and all other variables were maintained, the within-train facilitation in response to γ frequency stimulation was maintained in a manner analogous to our electrophysiological data (Fig. 9*F*, SD = 0.616).

Collectively, these findings indicate that the interaction between factors within the presynaptic terminal that govern vesicle release and recycling could underlie the low pass filter observed at the LPP–DG synapse. While the low pass filter may be described by a single set of presynaptic parameters, a combined response of low- and high-p synapses also provides a plausible explanation. When described by a single set of parameters, the simulated two-step model indicates that, in addition to release probability, subtle changes in the likelihood of the vesicles transitioning to the docked state may be an important factor.

Spaced bursts of gamma stimulation engage additional filtering

During complex behaviours it is common for entorhinal cortex neurons to emit short bursts of γ frequency activity riding on a slower θ wave (Chrobak et al., 2000). Such bursts are thought to improve the reliability of communication and to increase the signal to noise ratio (Lisman, 1997). Based on results described above, short bursts of two to three spikes could potentially reduce the impact of low pass filtering and exploit the initial frequency facilitation produced by θ stimulation. Such a scenario would enable the system to follow seconds-long spike trains that include γ frequency information. To test this idea, the LPP was stimulated using a $\theta\gamma$ pattern, involving a series of three pulse γ bursts separated by 200 ms. This strategy was only partially successful as LPP responses in the OML showed a noticeable within-train diminution of the composite potentials at burst intervals of 200 ms (Fig. 10*A* and *B*). This stands in contrast to the behaviour of CA3–CA1 synapses in which the net response to the fifth burst was larger than that to the first (Fig. 10*C* and *D*). Two factors contributed to the decrease in LPP burst responses: (1) relative to the initial LPP-evoked burst, the slope of the first fEPSP in each burst became progressively smaller over the course of the train and (2) the modest within-burst facilitation seen in the initial response was replaced by a within-burst depression (Fig. 10*B*, *E* and *F*). In CA1, the first response was enhanced rather than decreased throughout the five-burst train (Fig. 10*D* and *E*). We isolated the loss of frequency facilitation by normalizing within-burst slopes to the first response in each of the successive bursts. As shown, the modest facilitation seen in the first LPP response was greatly reduced on burst 2 and replaced by frequency depression on subsequent bursts (Fig. 10*F*); this occurred despite the reduction in the size of initial fEPSP in responses two through five. A loss of frequency facilitation was also evident in CA3–CA1 synapses when fEPSPs were normalized to the first (enhanced) potential in each burst (Fig. 10*F*).

Next, we investigated the time period over which between-burst depression of the initial response and suppression of within-burst facilitation operate. A burst-by-burst analysis indicated that a marked reduction in the first fEPSP slope was evident by the third burst response when using 200 ms intervals, but not when successive bursts were separated by either 1 or 5 s (Fig. 11*A* and *B*). Indeed, at interburst intervals of 1 and 5 s, responses were maintained, or at the longer interval moderately facilitated (relative to the initial fEPSP in the first burst), across bursts (Fig. 11*B*). However, the loss of within-burst facilitation with θ (i.e. 200 ms) interval spacing of bursts was still present when the interval between bursts was extended to 1 s, but not 5 s (Fig. 11*A* and *C*). These results indicate that short γ bursts engage surprisingly persistent mechanisms that add a second, novel type of filtering to the LPP–DG connection.

The duration of conventional IPSCs suggests that they do not play a significant role in the depression of spaced burst responses. However, γ frequency activation of the LPP produced GABAergic currents that persist for hundreds of milliseconds (see above). We tested if these prolonged currents affect interactions between bursts using PTX at a concentration (1 μM) that prolonged the decay phase (τ) of fEPSPs (122 ± 21.51%, $P = 0.0065$; paired Student's *t*-test) without causing after-discharges. PTX had no detectable effects on the slopes of the three fEPSPs in the first burst response but did partially offset the decrease in the first

fEPSP of subsequent bursts separated by 200 ms (Fig. 11*D* and *E*). The compound did not, however, detectably affect the loss of frequency facilitation that occurs within bursts during a $\theta\gamma$ stimulation train (Fig. 11*F*). In all, it appears that LPP $\theta\gamma$ bursts produce distinguishable effects on the initial fEPSP in subsequent bursts *vs.* frequency facilitation within those bursts. The first of these effects is less persistent than the second and is likely mediated by the unusual inhibition, possibly perisynaptic δ-$GABA_A$Rs, set in motion by a γ burst. The loss of frequency facilitation during a burst train is due to factors of another type.

Evidence that between-burst depression is due to presynaptic adjustments

Reducing extracellular Ca^{2+} had strong effects on responses to mixed frequency stimulation (i.e. $\theta\gamma$ train). As anticipated from the earlier experiment using 10-pulse γ trains, there was a marked facilitation of the second and third fEPSPs in the first burst response under conditions of reduced external Ca^{2+}, whereas the composite response to the fifth burst (200 ms delays) was clearly smaller (Fig. 12*A*). As described, a reduction of the first fEPSPs in each burst was one of two effects that emerged during a train of theta bursts under control conditions. Burst-by-burst analyses showed that this did not occur with 1 mM Ca^{2+} and instead the potentials were measurably larger relative to the first burst (Fig. 12*A* and *B*). This is not unexpected assuming that the lower Ca^{2+} concentration depresses LPP activation of, and subsequent release from, the GABAergic interneurons shown to contribute to the depression of first fEPSPs in PTX experiments described above. Frequency facilitation was present throughout the train, unlike the case with control Ca^{2+}, but became progressively smaller across successive bursts (Fig. 12*C*). This effect accounts for the depression of the net response to an LPP burst that is evident by burst no. 5 and suggests that the variables responsible for the depression of facilitation are not determined by release probability.

The persistent nature of the depression in frequency facilitation associated with $\theta\gamma$ stimulation suggests a mechanism with a long time course such as activation of postsynaptic SK channels. Infusion of apamin, which blocks these channels, in the presence of control levels of extracellular Ca^{2+} (2.5 mM) had minimal effects on the first burst response or on the reduction in the relative size of the response to the fifth burst (Fig. 13*A*). Quantitative analyses confirmed this and showed the progressive decrease in the responses during a train was still present, although modestly reduced in magnitude ($F_{(14,182)} = 2.459$, $P = 0.003$; Fig. 13*B*). Normalizing the slopes of the fEPSPs to the first potential in each burst response indicated that the loss of within-burst frequency facilitation was only slightly changed by apamin ($F_{(14,182)} = 1.873$, $P = 0.032$; Fig. 13*C*), an effect that was in stark contrast to the CA3–CA1 synapse and consistent with previous studies (Kramar et al., 2004). We conclude from this that SK channels do not make a significant contribution to the second of the carryover effects that occur between LPP $\theta\gamma$ bursts (i.e. the suppression of within burst facilitation).

Activation of apamin-insensitive intermediate conductance Ca^{2+}-dependent K^+ channels (i.e. $K_{Ca}3.1$) responsible for mediating the slow after-hyperpolarization (sAHP) that persists for seconds (Tiwari et al., 2018) may provide an alternative mechanism. To address this, we used the whole-cell voltage-clamp configuration to record LPP-evoked EPSCs (eEPSCs) from granule cells (V_{clamp} −50 mV) in the presence of the NMDAR and $GABA_A$R

antagonists AP-5 (50 μM) and bicuculline (20 μM), respectively. A potential contribution of postsynaptic Ca^{2+} to the impaired within-burst facilitation that occurs during a five-burst θγ train was tested by recording responses with and without the Ca^{2+} chelator BAPTA (10 mM) in the recording electrode internal solution. The suppression of responses, both across and within bursts, was largely unaffected by BAPTA in the recording electrode (Fig. 13*D–F*). These experiments support the conclusion from field recordings that $GABA_A$Rs do not make a significant contribution to the responses generated by theta bursts delivered to the LPP. Collectively, these findings suggest that the prolonged decrease in within-burst facilitation is not dependent upon postsynaptic Ca^{2+}-dependent mechanisms, but rather involves a process in the terminal that requires increased levels of the cation.

Discussion

Communication within and across nodes in brain circuits requires afferent inputs to efficiently drive output (i.e. action potential firing) from principal cells. As such the transformation of afferent inputs (i.e. amplification, filtering) across the synapse and how the subsequent response is processed along the somato-dendritic domain of the target cell are critical for determining information flow. At the level of the synapse, signal transformations involve the interaction between processes governing transmitter release (i.e. initial *p*, number of release sites) and those determining neurotransmitter and vesicle recycling (Edwards, 2007; Jackman & Regehr, 2017; Nanou & Catterall, 2018; Thomson, 2000), the net result being that synapses generally display facilitation or suppression of responses to inputs at behaviourally relevant frequencies (Thomson, 2000). Although there have been few planned comparisons between synaptic populations, it is evident from the literature that connections even within the same network respond in markedly different ways to the same pattern of afferent activation. For example, low frequency θ stimulation (5 Hz) is reported to produce within-train depression or various degrees of facilitation depending on where it is was applied in a seven-node circuit extending from the piriform cortex to hippocampal field CA1 (Trieu et al., 2015). Results of this kind strongly suggest that synapses are frequency ‘tuned’ according to their location, a factor that presumably shapes network level computations.

Results reported here indicate that the LPP–DG synapse expresses an unusual set of specialized features that interact in a frequency-specific manner to produce previously unsuspected types of synaptic filtering. Theta (5 Hz) LPP stimulation produced a slight degree of facilitation comparable to that recorded for CA3 to CA1 contacts, but γ (50 Hz) activation elicited a pattern unlike that reported for any other site in hippocampus: an initial facilitation followed by an overt suppression of the fEPSP. Together these features generate a type of low pass filter at one of the two pathways carrying cortical information to the first stage of hippocampal circuitry.

Synchronous discharges of the DG granule cells paralleled and exaggerated the changes in dendritic fEPSPs. The weak and sustained facilitation of fEPSPs during a 5 Hz train were converted into a dramatic enhancement of granule cell population spikes. In general, the number of contacts formed between any given group of axons and a population of target neurons in a sparse system (a given axon connects with a low percentage of target cells) without local topography will form a steep Poisson distribution with lowest values (fewest

synapses/neuron) to the left (Granger et al., 1989). Only a small percentage of the population will thus receive sufficient excitatory input to cross spike threshold. Facilitating release will allow the same sized input to drive the much larger group of near threshold neurons and thus produce a disproportionately (relative to the increase in fEPSP) greater increase in the number of responding neurons. Absent other factors, anatomical organization alone will serve to amplify input signals. But this argument also works in the reverse direction: a steadily developing depression of release will cause a much more rapid decline in the size of the population spike than of the fEPSP. In this sense, the same factors underlying amplification will sharpen low pass filtering as was observed here for β and γ frequency stimulation of the LPP.

Activation of the LPP with short γ bursts delivered at 200 ms intervals (i.e. theta burst stimulation), a behaviourally significant pattern of activity (Chrobak et al., 2000; Colgin, 2016), uncovered a second and complex set of filtering operations. The first response of the second and subsequent bursts in a train of five was depressed relative to that of the first burst. Furthermore, the within-burst facilitation declined across successive bursts. Together, these factors result in much reduced composite responses across successive theta bursts. The depression of frequency facilitation was long lasting in that it was still present when bursts were spaced apart by 1 s. In all, it appears that the LPP–DG connection faithfully relays, and indeed amplifies, θ pattern signals but potently depresses γ input whether arriving as a short train or as very brief bursts. The significance of these processes to circuit function depends on the manner in which the mossy fibre projections of the DG respond to activation at the two frequencies. The mossy fibre boutons exhibit an exaggerated form of frequency facilitation (Nicoll & Schmitz, 2005; Toth et al., 2000; Urban et al., 2001). If, as seems likely, this effect is greater at γ than θ frequencies, then low pass filtering by the LPP contacts could be seen as a device that prevents excessive mossy fibre activation of CA3 pyramidal neurons. These pyramidal cells generate a massive collateral feedback system capable of maintaining reverberating activity for remarkable periods (i.e. lasting minutes; Cox et al., 2019) and relatedly promote epileptiform discharges. There is also the possibility that the direct LPP input to CA3 does not follow the same rules as the LPP–DG connection (Breindl et al., 1994), in which case low pass filtering in the latter could serve to emphasize the importance of the former in processing γ frequency information (Fig. 14).

Postsynaptic mechanisms and the LPP–DG filter

We conducted a number of experiments to investigate the mechanisms underlying the unusual filtering of γ trains and $\theta\gamma$ bursts at LPP–DG synapses. The accumulation of feed-forward inhibition is an obvious candidate for the depression of dendritic and somatic (i.e. population spike) responses that emerges during these patterns. Although infusion of a low dose of the $GABA_AR$ antagonist PTX (1 μM) produced significant effects upon baseline responses, prolonging the fEPSP half-width and increasing the population spike amplitude, the within-train facilitation and suppression of both output measures remained intact. These findings indicate that feed-forward inhibition is critical for shaping the unitary fEPSP waveform and spike initiation dynamics but not the depression of responses across a γ train. Whole-cell voltage-clamp experiments using a saturating dose of PTX confirmed that the recruitment of feed-forward GABAergic transmission is not a critical determinant

of the within-train suppression observed during repetitive and burst patterns of stimulation. While this result may be somewhat surprising, factors associated with (1) the ability of interneurons to follow afferent inputs, (2) how the different experimental conditions (i.e. whole-cell *vs.* extracellular) influence the efficacy of $GABA_A$R-mediated inhibition and (3) the expression profile of $GABA_A$Rs need to be considered.

A number of prior studies have demonstrated that although DG interneurons are capable of firing at high frequencies in response to a persistent depolarizing current injection, or during paired interneuron–granule cell recordings, they do not reliably fire action potentials in response to perforant path stimulation (Ewell & Jones, 2010; Liu et al., 2014). This latter observation is critical when considering the operations of the local circuit. Our single-cell voltage-clamp data support such a scenario as the amplitude of LPP evoked IPSCs (eIPSCs) decreases in a frequency-dependent manner during brief stimulation trains, i.e. less interneurons spiking. Whether this is due to the LPP–interneuron synapse operating in a manner similar to the LPP–DG synapse described in the current study remains an interesting question.

The efficacy of $GABA_A$R-mediated inhibition, determined in large part by the activity of K–Cl co-transporter 2 (KCC2), in the extracellular recordings is also an important factor. Given that under physiological conditions the estimated driving force for Cl^- in granule cells is close to zero (Barmashenko et al., 2011; Goutierre et al., 2019), the size of $GABA_A$R-mediated currents will be significantly smaller than eIPSCs. As the DG contains high levels of δ-containing $GABA_A$Rs within the dentate gyrus, a receptor isoform located primarily at peri- and extrasynaptic sites that has a high affinity for GABA and very slow decay constants (Saxena & Macdonald, 1994; Sun et al., 2020), it is tempting to speculate that shunting inhibition dominates under basal conditions. The observation that partial PTX-mediated inhibition of $GABA_A$R function increased the population spike amplitude indicates that the local circuit is finely balanced and may reflect a reduction in δ-$GABA_A$R-mediated tonic inhibition (Wei et al., 2003). Such a PTX-induced change in spike initiation dynamics may mask any clear recruitment of feed-forward inhibition during brief periods of γ frequency activity. The transient inactivation of specific subpopulations of interneurons may be a useful approach to manipulate GABAergic transmission at this synapse.

The rapid activation (within 1 ms) and decay time course (200–400 ms) of SK channels (Adelman et al., 2012; Stocker, 2004) lend themselves to modulating responses generated by repetitive, high frequency inputs. Indeed, in CA1 the activation of SK2 channels by NMDAR-mediated increases in Ca^{2+} (Wang et al., 2014) has been shown to generate a conductance that significantly attenuates responses to CA3 inputs and elevates the threshold of LTP (Kramar et al., 2004; Ngo-Anh et al., 2005). Here we found inhibition of these Ca^{2+}-dependent channels, with apamin, had no significant effect upon the properties of baseline LPP-evoked fEPSPs, but did produce a small decrease in the within-train suppression of responses to γ frequency stimulation. A comparably modest effect was found for the within-train depression of $\theta\gamma$ burst responses. Given that SK channels are localized to the DG molecular layer (Sailer et al., 2004), it is tempting to postulate that the observed attenuation of responses to γ frequency stimulation are attributable to activation of these channels within the granule cell dendritic spines (Sailer et al., 2004). However,

intracellular administration of a Ca^{2+} chelator to DG granule cells, which would accordingly be anticipated to reduce activation of postsynaptic SK as well as the longer duration $K_{Ca}3.1$ (i.e. slow AHP) channels, had no detectable effect on within-train depression of theta burst responses. Thus, we conclude that, neither of two plausible postsynaptic mechanisms made major contributions to γ filtering at LPP synapses, suggesting the critical mechanisms are presynaptic.

The contribution of presynaptic factors to the LPP–DG filter

When considering potential factors present in the terminal that may contribute to the observed within-train suppression of responses, the temporal constraints imparted on the system, in this case by a 10-pulse γ train, are critical. Our data using low external Ca^{2+} levels indicate that the synaptic filtering at the LPP–DG synapse can largely be removed by reducing the initial *p*. A parsimonious interpretation of this observation is that lowering the initial *p* results in a reduction in the depletion of the RRP that occurs during repetitive, high frequency stimulation (Neher & Brose, 2018; Thomson, 2000). Current thinking posits that vesicular release is a sequential, two-step process, wherein vesicles are either 'loosely' or 'tightly' associated with the plasma membrane, such that only the latter are primed for rapid (microsecond time scale) transmitter release following local elevations in Ca^{2+} (Doussau et al., 2017; Miki et al., 2016, 2018; Neher & Brose, 2018; Pan & Zucker, 2009). Using Monte Carlo simulations of such a two-step model we were able to (1) investigate if presynaptic factors alone could recapitulate the experimental observations following γ frequency stimulation across three different synapses and (2) test how different factors such as release probability and RRP size influence the output curve. The two-step model, when constrained physiologically (e.g. initial *p*, number of docking sites, replacement vesicle number) was capable of recapitulating the output curves following γ frequency stimulation of CA3–CA1 (putative low *p* synapse), MPP–DG (putative high *p* synapse) and LPP–DG synapses. The simulation indicates that interaction between the initial *p* (i.e. δp_v) and replacement pool size (i.e. 'loose' vesicles) are critical determinants of the output curve. Specifically, reducing the size of the RRP decreased the simulated within-train facilitation observed at a low-*p* synapse and exaggerated the suppression evident at a high-*p* synapse. Finally, the observation that the LPP–DG synapse has the highest probability of vesicles transitioning to the docked state, a process that requires cytoskeletal changes (Miki et al., 2016), is intriguing given that plasticity at this synapse occurs via presynaptic mechanisms (Wang et al., 2016; Wang, Jia et al., 2018).

Vesicular glutamate transporters 1 and 2 (VGLUT1 and VGLUT2), the two primary brain variants, are expressed in a brain region-specific manner and ensure the refilling of vesicles with glutamate (Edwards, 2007; Fremeau et al., 2001). VGLUT1 is primarily found in cortex and is associated with frequency facilitation whereas VGLUT2 is enriched in subcortical and thalamocortical terminals and is typically associated with frequency depression (Fremeau et al., 2001, 2004; Fujiyama et al., 2001). The DG is unusual among cortical structures in that its molecular layer contains high concentrations of VGLUT2 (Halasy et al., 2004). Our experiments established that the transporter is present at high levels (relative to the CA3–CA1 system) in the LPP terminal field. We accordingly postulate that the LPP–DG synapse may represent a heterogeneous population of synapses,

comprising both low- and high-p synapses. In line with this view, combining the simulated output curves for putative low- (i.e. CA3–CA1) and high- (i.e. MPP–DG) p synapses was capable of recapitulating the LPP–DG low pass filter when an additional scale factor (i.e. weighted) was introduced with a ratio of 4:1 low- to high-p synapses. Remarkably, a weighted combination of the empirically measured output curves for the CA3–CA1 and MPP–DG responses also reproduced the low pass filter observed at the LPP–DG synapse. This suggests that the LPP–DG synapse has features common to both high- and low-p synapses, whilst the apparent differences in the ratios observed in the simulated and electrophysiological data likely result from comparing single synapse responses (i.e. simulation) and population responses at the level of the field potential.

While we posit that a depletion of the RRP associated with a preponderance of VGLUT2-containing terminals may be a primary factor for the initial suppression of responses during γ frequency inputs, there are a number of additional factors that merit consideration. First, our results indicate that levels of VGLUT1 and VGLUT2 do not differ between the LPP and MPP fields in DG, suggesting that the ratio of high- and low-p synapses is unlikely to explain the functional differences observed at these two synapses. The observation that the probability of vesicles transitioning to a docked state is ~20% higher at the simulated LPP–DG synapse may provide a clue that differences in cytoskeletal mobility are involved. In addition, it remains to be determined whether the different VGLUT isoforms are expressed in separate terminals, within the same terminal or even in the same synaptic vesicle. While it may be convenient to consider two distinct populations of terminals, the two isoforms have been identified within the same vesicle at the calyx of Held synapse (Nakakubo et al., 2020) and similar biphasic responses to high frequency stimulation have been observed at that contact (Taschenberger et al., 2016). A potentially important, as yet unexplored factor that may couple VGLUT isoforms with the apparent differences in synaptic filtering relates to whether the composition and spatial organization of the presynaptic active zone differs in a VGLUT-specific manner. Given the sensitivity of p to small changes in Ca^{2+} levels, the location and regulation of voltage-gated Ca^{2+} channels (VGCCs) within the active zone will be critical for regulating the efficacy of synaptic transmission (Dittman & Ryan, 2019; Thomson, 2000). While multiple mechanisms have been demonstrated to regulate VGCC function (Dolphin & Lee, 2020; Nanou & Catterall, 2018; Zamponi & Currie, 2013), our low Ca^{2+} data suggests that Ca^{2+}-dependent inactivation of these channels (DeMaria et al., 2001; Forsythe et al., 1998) is plausible at the LPP–DG synapse during γ frequency stimulation, in a manner analogous to processes identified in field CA1 (Nanou et al., 2018). Relatedly, the two-step model used here has a number of limitations when considered in the context of the current literature. First, presynaptic Ca^{2+} concentrations are not dynamic such that intra-terminal concentrations of the cation, and as a result the initial p, can vary across subsequent inputs. This has implications when considering that loosely associated vesicles may contribute to synaptic transmission by rapidly transitioning (1–5 ms) to the primed, tightly associated state, from which neurotransmitter release can occur when presynaptic Ca^{2+} levels are high (Miki et al., 2018). In addition to having a greater proportion of vesicles in the primed state initially, high-p synapses also exhibit a prevalence to incorporate loosely associated vesicles during repetitive activation (Miki et al., 2018; Neher & Brose, 2018), a feature that has significant implications for their operations during high frequency

stimulation. Such a rapid transition of loosely associated vesicles will not only increase the latency to synaptic release (decreasing temporal precision), but also introduce a refractory period (30–50 ms) earlier in the train as they are replenished (Miki et al., 2018; Neher & Brose, 2018; Thomson, 2000). Regarding the latter point, recent evidence indicates the replenishment pool, upstream of the RRP, is small in size and as such its depletion during repetitive stimulation is likely to significantly influence synaptic responses (Tran et al., 2022), a factor not considered in the current simulations.

The above arguments suggest a reasonable framework for explaining the filtering of γ trains by the LPP, although it seems unlikely that they will account for the seconds-long period over which theta bursts are depressed during repetitive administration. Reducing extracellular Ca^{2+} restored within-burst frequency facilitation but with a magnitude that became progressively smaller across successive bursts, suggesting that the factors responsible for eliminating facilitation under control conditions were still operative. A simplistic interpretation may be that lowering external Ca^{2+} reduces the initial p sufficiently at high-p synapses (i.e. VGLUT2) such that these synapses now primarily display classic frequency facilitation and RRP depletion does not occur. However, the notion that depletion of the RRP associated with high-p synapses could explain the suppression observed across successive bursts separated by 200 ms appears unlikely given the proposed rates of vesicle trafficking to the membrane (30–50 ms). An alternative explanation may relate to mechanisms thought to underlie the Ca^{2+}-dependent transition of loosely associated vesicles to replenish the primed vesicle pool that influence release dynamics. The activity of Munc13 family proteins, critical for vesicle priming, is regulated by multiple Ca^{2+}-dependent processes (Junge et al., 2004; Shin et al., 2010), while latrunculin-sensitive cytoskeletal changes are additionally required for this transition of vesicles to a primed state (Miki et al., 2016, 2018). The latter is intriguing as long-term potentiation at the LPP–DG synapse is expressed presynaptically, and is dependent upon atypical endocannabinoid signalling that initiates cytoskeletal changes via activation of focal adhesion kinase (FAK) and β1 integrin signalling (Wang et al., 2016; Wang, Jia et al., 2018). Although speculative, this suggests the hypothesis that the LPP terminals are highly dynamic structures where bursts of afferent inputs (i.e. $\theta\gamma$ bursts) are capable of initiating cytoskeletal alterations within the terminal that influences the organization of the active zone so that release is impaired. Such alterations in the presynaptic cytoskeleton would be anticipated to persist for seconds, as experimentally observed.

Supplementary Material

Refer to Web version on PubMed Central for supplementary material.

Acknowledgements

The authors would like to thank Dr Alain Marty and Dr Takafumi Miki for providing the simulated two-step model and their advice on its use.

Funding

This work was supported in part by NIH grant MH101491 (to G.L.), NIH NIDA P50 grant DA044118 (to C.M.G. and G.L.), NIH NICHD grant RHD089491A (to C.M.G. and G.L.) and ONR grants N00014–18-1–2114

and N00014–21-1–2940 (to G.L.). J.Q. was supported by the National Science Foundation Graduate Research Fellowship under Grant No. DGE-1839285.

Biography

Julian Quintanilla received his bachelor's degree in Neurobiology from the University of California, Irvine. Because of his interest in the cellular aspects of learning and memory, he joined the Interdepartmental Graduate Program at the University of California, Irvine and is currently a PhD candidate within the department of Anatomy & Neurobiology. His research interest looks at hippocampal processing, specifically at the two termination sites of the lateral perforant path of the lateral entorhinal cortex, the dentate gyrus and field CA3.

Data availability statement

Data and modelling code are available upon request to the corresponding author.

References

Adelman JP, Maylie J, & Sah P. (2012). Small-conductance Ca^{2+}-activated K^{+} channels: Form and function. Annual Review of Physiology, 74(1), 245–269.

Amani M, Lauterborn JC, Le AA, Cox BM, Wang W, Quintanilla J, Cox CD, Gall CM, & Lynch G. (2021). Rapid aging in the perforant path projections to the rodent dentate gyrus. Journal of Neuroscience, 41(10), 2301–2312. [PubMed: 33514675]

Arai A, Silberg J, & Lynch G. (1995). Differences in the refractory properties of two distinct inhibitory circuitries in field CA1 of the hippocampus. Brain Research, 704(2), 298–306. [PubMed: 8788926]

Barmashenko G, Hefft S, Aertsen A, Kirschstein T, & Kohling R. (2011). Positive shifts of the GABAA receptor reversal potential due to altered chloride homeostasis is widespread after status epilepticus. Epilepsia, 52(9), 1570–1578. [PubMed: 21899534]

Bellocchio EE, Hu HL, Pohorille A, Chan J, Pickel VM, & Edwards RH. (1998). The localization of the brain-specific inorganic phosphate transporter suggests a specific presynaptic role in glutamatergic transmission. Journal of Neuroscience, 18(21), 8648–8659. [PubMed: 9786972]

Bough KJ, Mott DD, & Dingledine RJ. (2004). Medial perforant path inhibition mediated by mGluR7 is reduced after status epilepticus. Journal of Neurophysiology, 92(3), 1549–1557. [PubMed: 15152022]

Bragin A, Jando G, Nadasdy Z, Hetke J, Wise K, & Buzsaki G. (1995). Gamma (40–100 Hz) oscillation in the hippocampus of the behaving rat. Journal of Neuroscience, 15(1), 47–60. [PubMed: 7823151]

Breindl A, Derrick BE, Rodriguez SB, & Martinez JL Jr, (1994). Opioid receptor-dependent long-term potentiation at the lateral perforant path-CA3 synapse in rat hippocampus. Brain Research Bulletin, 33(1), 17–24. [PubMed: 8275323]

Chen LY, Rex CS, Sanaiha Y, Lynch G, & Gall CM. (2010). Learning induces neurotrophin signaling at hippocampal synapses. Proceedings of the National Academy of Sciences, USA, 107(15), 7030–7035.

Christie BR, & Abraham WC. (1994). Differential regulation of paired-pulse plasticity following LTP in the dentate gyrus. Neuroreport, 5(4), 385–388. [PubMed: 8003660]

Chrobak JJ, & Buzsaki G. (1998). Gamma oscillations in the entorhinal cortex of the freely behaving rat. Journal of Neuroscience, 18(1), 388–398. [PubMed: 9412515]

Chrobak JJ, Lorincz A, & Buzsaki G. (2000). Physiological patterns in the hippocampo-entorhinal cortex system. Hippocampus, 10(4), 457–465. [PubMed: 10985285]

Colgin LL. (2015). Theta-gamma coupling in the entorhinal-hippocampal system. Current Opinion in Neurobiology, 31, 45–50. [PubMed: 25168855]

Colgin LL. (2016). Rhythms of the hippocampal network. Nature Reviews. Neuroscience, 17(4), 239–249. [PubMed: 26961163]

Colgin LL, Denninger T, Fyhn M, Hafting T, Bonnevie T, Jensen O, Moser MB, & Moser EI. (2009). Frequency of gamma oscillations routes flow of information in the hippocampus. Nature, 462(7271), 353–357. [PubMed: 19924214]

Cox BM, Cox CD, Gunn BG, Le AA, Inshishian VC, Gall CM, & Lynch G. (2019). Acquisition of temporal order requires an intact CA3 commissural/associational (C/A) feedback system in mice. Communications Biology, 2(1), 251. [PubMed: 31286068]

Davies CH, Starkey SJ, Pozza MF, & Collingridge GL. (1991). GABA autoreceptors regulate the induction of LTP. Nature, 349(6310), 609–611. [PubMed: 1847993]

DeMaria CD, Soong TW, Alseikhan BA, Alvania RS, & Yue DT. (2001). Calmodulin bifurcates the local Ca^{2+} signal that modulates P/Q-type Ca^{2+} channels. Nature, 411(6836), 484–489. [PubMed: 11373682]

Dittman JS, & Ryan TA. (2019). The control of release probability at nerve terminals. Nature Reviews. Neuroscience, 20(3), 177–186. [PubMed: 30647451]

Dolorfo CL, & Amaral DG. (1998). Entorhinal cortex of the rat: Topographic organization of the cells of origin of the perforant path projection to the dentate gyrus. Journal of Comparative Neurology, 398(1), 25–48. [PubMed: 9703026]

Dolphin AC, & Lee A. (2020). Presynaptic calcium channels: Specialized control of synaptic neurotransmitter release. Nature Reviews. Neuroscience, 21(4), 213–229. [PubMed: 32161339]

Doussau F, Schmidt H, Dorgans K, Valera AM, Poulain B, & Isope P. (2017). Frequency-dependent mobilization of heterogeneous pools of synaptic vesicles shapes presynaptic plasticity. eLife, 6, e28935.

Eccles JC, Katz B, & Kuffler SW. (1941). Nature of the “endplate potential” in curarized muscle. Journal of Neurophysiology, 4(5), 362–387.

Edwards RH. (2007). The neurotransmitter cycle and quantal size. Neuron, 55(6), 835–858. [PubMed: 17880890]

Ewell LA, & Jones MV. (2010). Frequency-tuned distribution of inhibition in the dentate gyrus. Journal of Neuroscience, 30(38), 12597–12607.

Forsythe ID, Tsujimoto T, Barnes-Davies M, Cuttle MF, & Takahashi T. (1998). Inactivation of presynaptic calcium current contributes to synaptic depression at a fast central synapse. Neuron, 20(4), 797–807. [PubMed: 9581770]

Fremeau RT, Kam K, Qureshi T, Johnson J, Copenhagen DR, Storm-Mathisen J, Chaudhry FA, Nicoll RA, & Edwards RH. (2004). Vesicular glutamate transporters 1 and 2 target to functionally distinct synaptic release sites. Science, 304(5678), 1815–1819. [PubMed: 15118123]

Fremeau RT, Troyer MD, Pahner I, Nygaard GO, Tran CH, Reimer RJ, Bellocchio EE, Fortin D, Storm-Mathisen J, & Edwards RH. (2001). The expression of vesicular glutamate transporters defines two classes of excitatory synapse. Neuron, 31(2), 247–260. [PubMed: 11502256]

Fujiyama F, Furuta T, & Kaneko T. (2001). Immunocytochemical localization of candidates for vesicular glutamate transporters in the rat cerebral cortex. Journal of Comparative Neurology, 435(3), 379–387. [PubMed: 11406819]

Goutierre M, Al Awabdh S, Donneger F, Francois E, Gomez-Dominguez D, Irinopoulou T, Menendez de la Prida L, & Poncer JC. (2019). KCC2 regulates neuronal excitability and hippocampal activity via interaction with task-3 channels. Cell Reports, 28(1), 91–103.e7.

Granger R, Ambros-Ingerson J, & Lynch G. (1989). Derivation of encoding characteristics of layer II cerebral cortex. Journal of Cognitive Neuroscience, 1(1), 61–87. [PubMed: 23968411]

Gunn BG, Cox CD, Chen Y, Frotscher M, Gall CM, Baram TZ, & Lynch G. (2017). The endogenous stress hormone CRH modulates excitatory transmission and network physiology in hippocampus. Cerebral Cortex, 27(8), 4182–4198. [PubMed: 28460009]

Guthrie KM, Nguyen T, & Gall CM. (1995). Insulin-like growth factor-1 mRNA is increased in deafferented hippocampus: Spatiotemporal correspondence of a trophic event with axon sprouting. The Journal of Comparative Neurology, 352(1), 147–160. [PubMed: 7714238]

Halasy K, Hajszan T, Kovacs EG, Lam TT, & Leranth C. (2004). Distribution and origin of vesicular glutamate transporter 2-immunoreactive fibers in the rat hippocampus. Hippocampus, 14(7), 908–918. [PubMed: 15382259]

Hargreaves EL, Rao G, Lee I, & Knierim JJ. (2005). Major dissociation between medial and lateral entorhinal input to dorsal hippocampus. Science, 308(5729), 1792–1794. [PubMed: 15961670]

Herzog E, Gilchrist J, Gras C, Muzerelle A, Ravassard P, Giros B, Gaspar P, & El Mestikawy S. (2004). Localization of VGLUT3, the vesicular glutamate transporter type 3, in the rat brain. Neuroscience, 123(4), 983–1002. [PubMed: 14751290]

Hjorth-Simonsen A. (1972). Projection of the lateral part of the entorhinal area to the hippocampus and fascia dentata. Journal of Comparative Neurology, 146(2), 219–231. [PubMed: 5073889]

Jackman SL, & Regehr WG. (2017). The mechanisms and functions of synaptic facilitation. Neuron, 94(3), 447–464. [PubMed: 28472650]

Jackman SL, Turecek J, Belinsky JE, & Regehr WG. (2016). The calcium sensor synaptotagmin 7 is required for synaptic facilitation. Nature, 529(7584), 88. [PubMed: 26738595]

Jensen O, & Colgin LL. (2007). Cross-frequency coupling between neuronal oscillations. Trends in Cognitive Sciences, 11(7), 267–269. [PubMed: 17548233]

Junge HJ, Rhee JS, Jahn O, Varoqueaux F, Spiess J, Waxham MN, Rosenmund C, & Brose N. (2004). Calmodulin and Munc13 form a Ca^{2+} sensor/effector complex that controls short-term synaptic plasticity. Cell, 118(3), 389–401. [PubMed: 15294163]

Kaneko T, Fujiyama F, & Hioki H. (2002). Immunohistochemical localization of candidates for vesicular glutamate transporters in the rat brain. Journal of Comparative Neurology, 444(1), 39–62. [PubMed: 11835181]

Katz B, & Miledi R. (1968). Role of calcium in neuromuscular facilitation. Journal of Physiology, 195, 481. [PubMed: 4296699]

Koutsoumpa A, & Papatheodoropoulos C. (2019). Short-term dynamics of input and output of CA1 network greatly differ between the dorsal and ventral rat hippocampus. BMC Neuroscience, 20, 35. [PubMed: 31331291]

Kramar EA, Lin B, Lin CY, Arai AC, Gall CM, & Lynch G. (2004). A novel mechanism for the facilitation of theta-induced long-term potentiation by brain-derived neurotrophic factor. Journal of Neuroscience, 24(22), 5151–5161. [PubMed: 15175384]

Larson J, & Lynch G. (1986). Induction of synaptic potentiation in hippocampus by patterned stimulation involves two events. Science, 232(4753), 985–988. [PubMed: 3704635]

Larson J, & Munkacsy E. (2015). Theta-burst LTP. Brain Research, 1621, 38–50. [PubMed: 25452022]

Lauterborn JC, Scaduto P, Cox CD, Schulmann A, Lynch G, Gall CM, Keene CD, & Limon A. (2021). Increased excitatory to inhibitory synaptic ratio in parietal cortex samples from individuals with Alzheimer's disease. Nature Communications, 12(1), 2603.

Le AA, Lauterborn JC, Jia Y, Wang W, Cox CD, Gall CM, & Lynch G. (2022). Prepubescent female rodents have enhanced hippocampal LTP and learning relative to males, reversing in adulthood as inhibition increases. Nature Neuroscience, 25(2), 180–190. [PubMed: 35087246]

Lisman JE. (1997). Bursts as a unit of neural information: Making unreliable synapses reliable. Trends in Neurosciences, 20(1), 38–43. [PubMed: 9004418]

Liu YC, Cheng JK, & Lien CC. (2014). Rapid dynamic changes of dendritic inhibition in the dentate gyrus by presynaptic activity patterns. Journal of Neuroscience, 34(4), 1344–1357. [PubMed: 24453325]

Lynch G, Matthews DA, Mosko S, Parks T, & Cotman C. (1972). Induced acetylcholinesterase-rich layer in rat dentate gyrus following entorhinal lesions. Brain Research, 42(2), 311–318. [PubMed: 4115093]

Macek TA, Winder DG, Gereau RWT, Ladd CO, & Conn PJ. (1996). Differential involvement of group II and group III mGluRs as autoreceptors at lateral and medial perforant path synapses. Journal of Neurophysiology, 76(6), 3798–3806. [PubMed: 8985877]

McNaughton BL. (1980). Evidence for two physiologically distinct perforant pathways to the fascia dentata. Brain Research, 199(1), 1–19. [PubMed: 7407615]

McNaughton BL. (1982). Long-term synaptic enhancement and short-term potentiation in rat fascia dentata act through different mechanisms. Journal of Physiology, 324(1), 249–262. [PubMed: 7097600]

Miki T, Malagon G, Pulido C, Llano I, Neher E, & Marty A. (2016). Actin- and myosin-dependent vesicle loading of presynaptic docking sites prior to exocytosis. Neuron, 91(4), 808–823. [PubMed: 27537485]

Miki T, Nakamura Y, Malagon G, Neher E, & Marty A. (2018). Two-component latency distributions indicate two-step vesicular release at simple glutamatergic synapses. Nature Communications, 9(1), 3943.

Mott DD, & Lewis DV. (1991). Facilitation of the induction of long-term potentiation by GABAB receptors. Science, 252(5013), 1718–1720. [PubMed: 1675489]

Nakakubo Y, Abe S, Yoshida T, Takami C, Isa M, Wojcik SM, Brose N, Takamori S, & Hori T. (2020). Vesicular glutamate transporter expression ensures high-fidelity synaptic transmission at the calyx of held synapses. Cell Reports, 32(7), 108040.

Nanou E, & Catterall WA. (2018). Calcium channels, synaptic plasticity, and neuropsychiatric disease. Neuron, 98(3), 466–481. [PubMed: 29723500]

Nanou E, Lee A, & Catterall WA. (2018). Control of excitation/inhibition balance in a hippocampal circuit by calcium sensor protein regulation of presynaptic calcium channels. Journal of Neuroscience, 38(18), 4430–4440. [PubMed: 29654190]

Neher E, & Brose N. (2018). Dynamically primed synaptic vesicle states: Key to understand synaptic short-term plasticity. Neuron, 100(6), 1283–1291. [PubMed: 30571941]

Ngo-Anh TJ, Bloodgood BL, Lin M, Sabatini BL, Maylie J, & Adelman JP. (2005). SK channels and NMDA receptors form a Ca^{2+}-mediated feedback loop in dendritic spines. Nature Neuroscience, 8(5), 642–649. [PubMed: 15852011]

Nicoll RA, & Schmitz D. (2005). Synaptic plasticity at hippocampal mossy fibre synapses. Nature Reviews. Neuroscience, 6(11), 863–876. [PubMed: 16261180]

Nusser Z, Sieghart W, & Somogyi P. (1998). Segregation of different GABAA receptors to synaptic and extrasynaptic membranes of cerebellar granule cells. Journal of Neuroscience, 18(5), 1693–1703. [PubMed: 9464994]

Pacelli GJ, Su W, & Kelso SR. (1989). Activity-induced depression of synaptic inhibition during LTP-inducing patterned stimulation. Brain Research, 486(1), 26–32. [PubMed: 2720432]

Pan B, & Zucker RS. (2009). A general model of synaptic transmission and short-term plasticity. Neuron, 62(4), 539–554. [PubMed: 19477155]

Reagh ZM, & Yassa MA. (2014). Object and spatial mnemonic interference differentially engage lateral and medial entorhinal cortex in humans. Proceedings of the National Academy of Sciences, USA, 111, E4264–4273.

Rex CS, Chen LY, Sharma A, Liu J, Babayan AH, Gall CM, & Lynch G. (2009). Different Rho GTPase-dependent signaling pathways initiate sequential steps in the consolidation of long-term potentiation. Journal of Cell Biology, 186(1), 85–97. [PubMed: 19596849]

Rohde J, Kirschstein T, Wilkars W, Muller L, Tokay T, Porath K, Bender RA, & Kohling R. (2012). Upregulation of presynaptic mGluR2, but not mGluR3 in the epileptic medial perforant path. Neuropharmacology, 62(4), 1867–1873. [PubMed: 22202905]

Sailer CA, Kaufmann WA, Marksteiner J, & Knaus HG. (2004). Comparative immunohistochemical distribution of three small-conductance Ca^{2+}-activated potassium channel subunits, SK1, SK2, and SK3 in mouse brain. Molecular and Cellular Neurosciences, 26(3), 458–469. [PubMed: 15234350]

Saxena NC, & Macdonald RL. (1994). Assembly of GABAA receptor subunits: role of the delta subunit. Journal of Neuroscience, 14(11), 7077–7086. [PubMed: 7525894]

Seese RR, Chen LY, Cox CD, Schulz D, Babayan AH, Bunney WE, Henn FA, Gall CM, & Lynch G. (2013). Synaptic abnormalities in the infralimbic cortex of a model of congenital depression. Journal of Neuroscience, 33(33), 13441–13448.

Seese RR, Wang K, Yao YQ, Lynch G, & Gall CM. (2014). Spaced training rescues memory and ERK1/2 signaling in fragile X syndrome model mice. Proceedings of the National Academy of Sciences, USA, 111(47), 16907–16912.

Shin OH, Lu J, Rhee JS, Tomchick DR, Pang ZP, Wojcik SM, Camacho-Perez M, Brose N, Machius M, Rizo J, Rosenmund C, & Sudhof TC. (2010). Munc13 C2B domain is an activity-dependent Ca^{2+} regulator of synaptic exocytosis. Nature Structural & Molecular Biology, 17, 280–288.

Steward O. (1976). Topographic organization of the projections from the entorhinal area to the hippocampal formation of the rat. Journal of Comparative Neurology, 167(3), 285–314. [PubMed: 1270625]

Stocker M. (2004). Ca(2+)-activated K^+ channels: Molecular determinants and function of the SK family. Nature Reviews. Neuroscience, 5(10), 758–770. [PubMed: 15378036]

Sun MY, Ziolkowski L, & Mennerick S. (2020). Delta subunit-containing GABAA IPSCs are driven by both synaptic and diffusional GABA in mouse dentate granule neurons. Journal of Physiology, 598(6), 1205–1221. [PubMed: 31951019]

Taschenberger H, Woehler A, & Neher E. (2016). Super-priming of synaptic vesicles as a common basis for inter-synapse variability and modulation of synaptic strength. Proceedings of the National Academy of Sciences, USA, 113, E4548–E4557.

Thomson AM. (2000). Facilitation, augmentation and potentiation at central synapses. Trends in Neurosciences, 23(7), 305–312. [PubMed: 10856940]

Tiwari MN, Mohan S, Biala Y, & Yaari Y. (2018). Differential contributions of Ca2+ -activated K+ channels and Na(+) /K(+)-ATPases to the generation of the slow afterhyperpolarization in CA1 pyramidal cells. Hippocampus, 28(5), 338–357. [PubMed: 29431274]

Tort AB, Komorowski RW, Manns JR, Kopell NJ, & Eichenbaum H. (2009). Theta-gamma coupling increases during the learning of item-context associations. Proceedings of the National Academy of Sciences, USA, 106(49), 20942–20947.

Toth K, Suares G, Lawrence JJ, Philips-Tansey E, & McBain CJ. (2000). Differential mechanisms of transmission at three types of mossy fiber synapse. Te Journal of Neuroscience, 20(22), 8279–8289.

Tran V, Miki T, & Marty A. (2022). Three small vesicular pools in sequence govern synaptic response dynamics during action potential trains. Proceedings of the National Academy of Sciences, USA, 119(5), e2114469119.

Trieu BH, Kramar EA, Cox CD, Jia YS, Wang WS, Gall CM, & Lynch G. (2015). Pronounced differences in signal processing and synaptic plasticity between piriform-hippocampal network stages: A prominent role for adenosine. Journal of Physiology, 593(13), 2889–2907. [PubMed: 25902928]

Tsao A, Moser MB, & Moser EI. (2013). Traces of experience in the lateral entorhinal cortex. Current Biology, 23(5), 399–405. [PubMed: 23434282]

Urban NN, Henze DA, & Barrionuevo G. (2001). Revisiting the role of the hippocampal mossy fiber synapse. Hippocampus, 11(4), 408–417. [PubMed: 11530845]

Wang K, Lin MT, Adelman JP, & Maylie J. (2014). Distinct Ca^{2+} sources in dendritic spines of hippocampal CA1 neurons couple to SK and Kv4 channels. Neuron, 81(2), 379–387. [PubMed: 24462100]

Wang W, Cox BM, Jia Y, Le AA, Cox CD, Jung KM, Hou B, Piomelli D, Gall CM, & Lynch G. (2018). Treating a novel plasticity defect rescues episodic memory in Fragile X model mice. Molecular Psychiatry, 23(8), 1798–1806. [PubMed: 29133950]

Wang W, Jia Y, Pham DT, Palmer LC, Jung KM, Cox CD, Rumbaugh G, Piomelli D, Gall CM, & Lynch G. (2018). Atypical endocannabinoid signaling initiates a new form of memory-related plasticity at a cortical input to hippocampus. Cerebral Cortex, 28(7), 2253–2266. [PubMed: 28520937]

Wang W, Le AA, Hou B, Lauterborn JC, Cox CD, Levin ER, Lynch G, & Gall CM. (2018). Memory-related synaptic plasticity is sexually dimorphic in rodent hippocampus. Journal of Neuroscience, 38(37), 7935–7951. [PubMed: 30209204]

Wang WS, Trieu BH, Palmer LC, Jia YS, Pham DT, Jung KM, Karsten CA, Merrill CB, Mackie K, Gall CM, Piomelli D, & Lynch G. (2016). A primary cortical input to hippocampus expresses a pathway-specific and endocannabinoid-dependent form of long-term potentiation. eNeuro, 3(4), ENEURO.0160–16.2016.

Wei W, Zhang N, Peng Z, Houser CR, & Mody I. (2003). Perisynaptic localization of delta subunit-containing GABA(A) receptors and their activation by GABA spillover in the mouse dentate gyrus. Journal of Neuroscience, 23(33), 10650–10661. [PubMed: 14627650]

Weston MC, Nehring RB, Wojcik SM, & Rosenmund C. (2011). Interplay between VGLUT isoforms and endophilin A1 regulates neurotransmitter release and short-term plasticity. Neuron, 69(6), 1147–1159. [PubMed: 21435559]

Witter MP. (1993). Organization of the entorhinal hippocampal system – A review of current anatomical data. Hippocampus, 3(S1), 33–44. [PubMed: 8287110]

Yoganarasimha D, Rao G, & Knierim JJ. (2011). Lateral entorhinal neurons are not spatially selective in cue-rich environments. Hippocampus, 21,12, 1363–1374. [PubMed: 20857485]

Zamponi GW, & Currie KP. (2013). Regulation of Ca(V)2 calcium channels by G protein coupled receptors. Biochimica et Biophysica Acta, 1828(7), 1629–1643. [PubMed: 23063655]

Key points

- The lateral perforant path (LPP)–dentate gyrus (DG) synapse operates as a low-pass filter, where responses to a train of 50 Hz, γ frequency activation are greatly suppressed.
- Activation with brief bursts of γ frequency information engages a secondary filter that persists for prolonged periods (lasting seconds).
- Both forms of LPP frequency filtering are influenced by presynaptic, as opposed to postsynaptic, processes; this contrasts with other hippocampal synapses.
- LPP frequency filtering is modified by the unique presynaptic long-term potentiation at this synapse.
- Computational simulations indicate that presynaptic factors associated with release probability and vesicle recycling may underlie the potent LPP–DG frequency filtering.

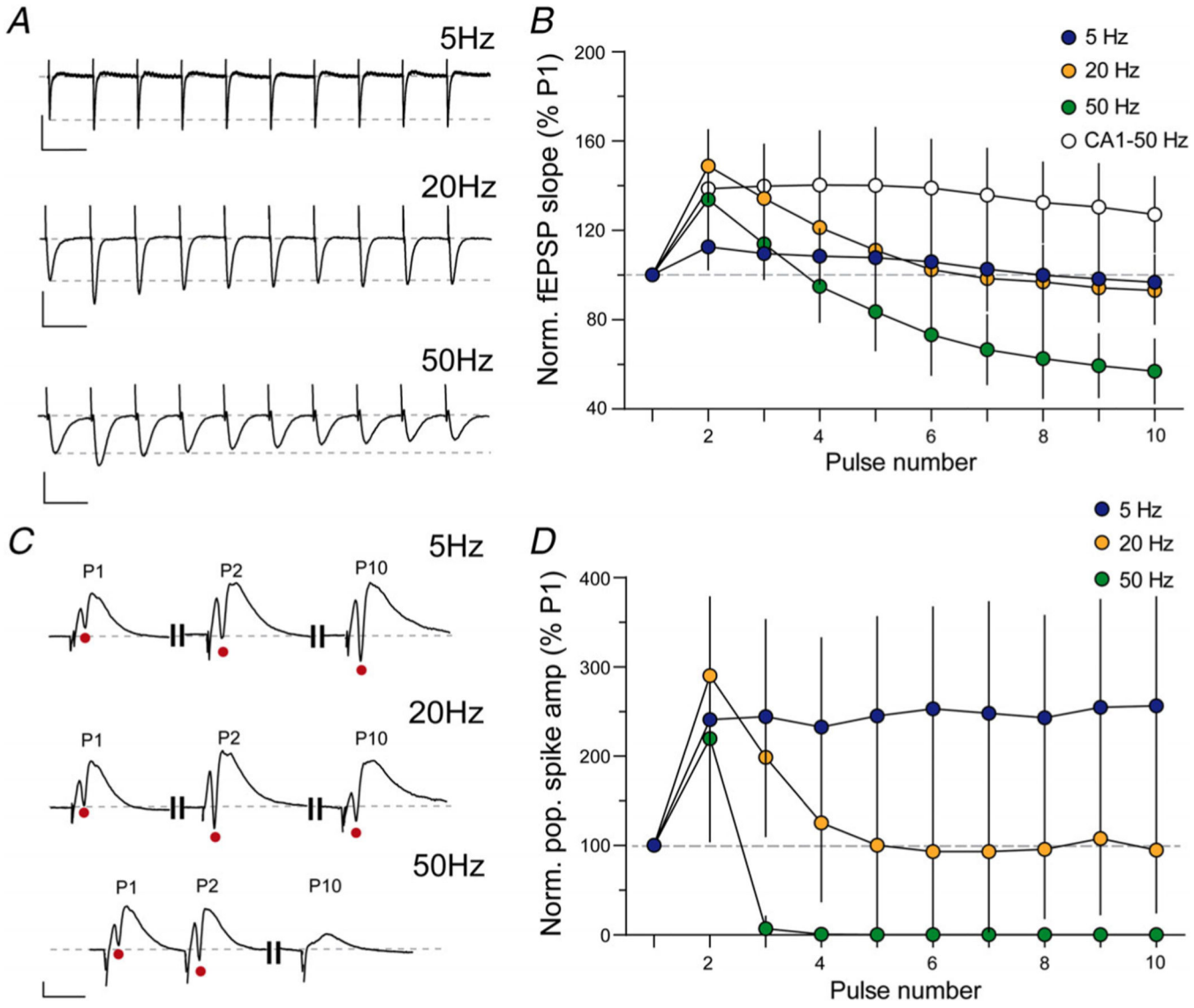

Figure 1. The LPP–DG synapse operates as a low pass filter

A, representative traces recorded from the DG OML in response to LPP stimulation with 10 pulse trains delivered at 5, 20 and 50 Hz (scale bars: 5 Hz: $y = 1$ mV, $x = 200$ ms; 20 Hz: $y = 1$ mV, $x = 50$ ms; 50 Hz: $y = 1$ mV, $x = 20$ ms). *B*, graph summarizing the within-train facilitation of the fEPSP slope for each stimulation frequency. Note the striking difference in the nature of the responses generated at LPP–DG (green circles) and CA3–CA1 (white circles) synapses following stimulation at 50 Hz (for all frequencies, $n = 21$–22 slices/9 animals). *C*, representative traces showing the first two and final responses recorded from the granule cell layer with a 10-pulse stimulation train delivered to the LPP at 5, 20 and 50 Hz. The stimulation intensity was increased to generate a small population spike (red circles; scale bars: $y = 1$ mV, $x = 10$ ms). *D*, graph summarizing the within-train facilitation of the population amplitude for each stimulation frequency (5 and 20 Hz, $n = 7$ slices; 50 Hz, $n = 10$ slices; $n = 4$ mice per frequency). Note the extreme filtering of spike output at frequencies in the γ (50 Hz) range.

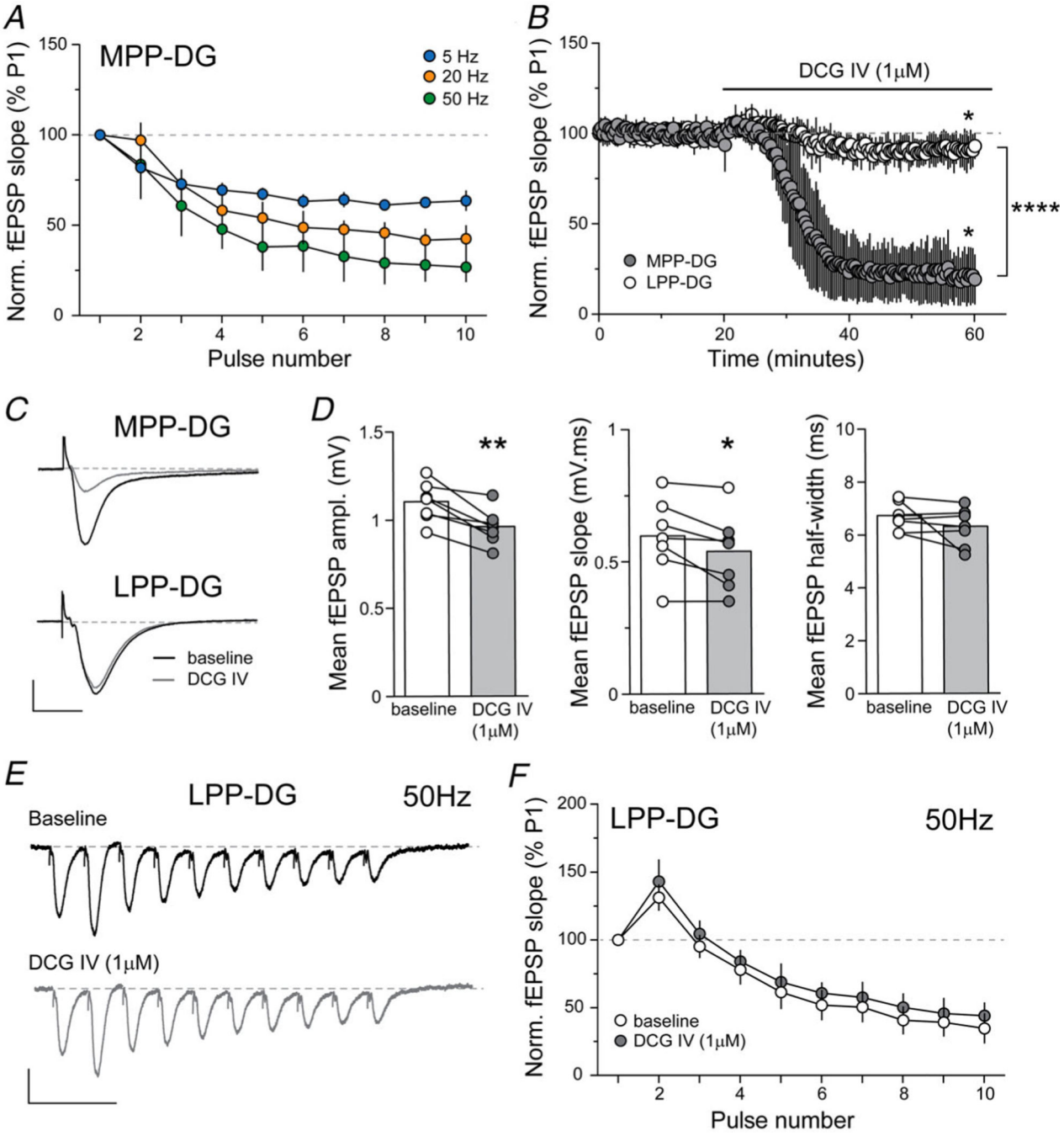

Figure 2. Low pass filtering at the LPP–DG synapse is independent of MPP inputs

A, graph summarizing the fEPSP slope responses of the MPP reveals a depression across all three frequency trains (5, 20 and 50 Hz). *B*, infusion of the mGluRII agonist DCG IV (1 μM) markedly depressed baseline MPP fEPSPs (MPP: $t_2 = 9.88$, $^*P = 0.01$, average of the last 5 min before and after infusion). DCG IV infusion has much smaller effects on LPP–DG fEPSPs (LPP: $t_6 = 3.18$, $^*P = 0.02$; MPP *vs.* LPP: $t_8 = 9.6$, $^{****}P < 0.0001$; LPP $n = 7$ slices/5 mice; MPP $n = 3$ slices/2 mice, unpaired Student's *t*-test of the average of the last 5 min). *C*, representative traces of MPP–DG (top) and LPP–DG (bottom) responses

before (black) and after (grey) DCG IV infusion. *D*, summary graphs showing the effects of DCG IV on LPP–DG fEPSP amplitude (** $P = 0.004$, paired *t*-test), slope (* $P = 0.028$) and half-width ($P = 0.209$) for individual slices ($n = 7$ slices/5 mice). *E*, representative traces recorded from the OML of the DG in response to LPP stimulation with a 10 pulse 50 Hz train before (black) and 40 min after (grey) bath application of DCG IV (1 μM). *F*, the within-train depression of fEPSP slopes of LPP–DG synapses at 50 Hz was not influenced by 40 min DCG IV infusion ($F_{(9,54)} = 1.06$, $P = 0.41$; $n = 7$ slices/mice per group; two way RM-ANOVA).

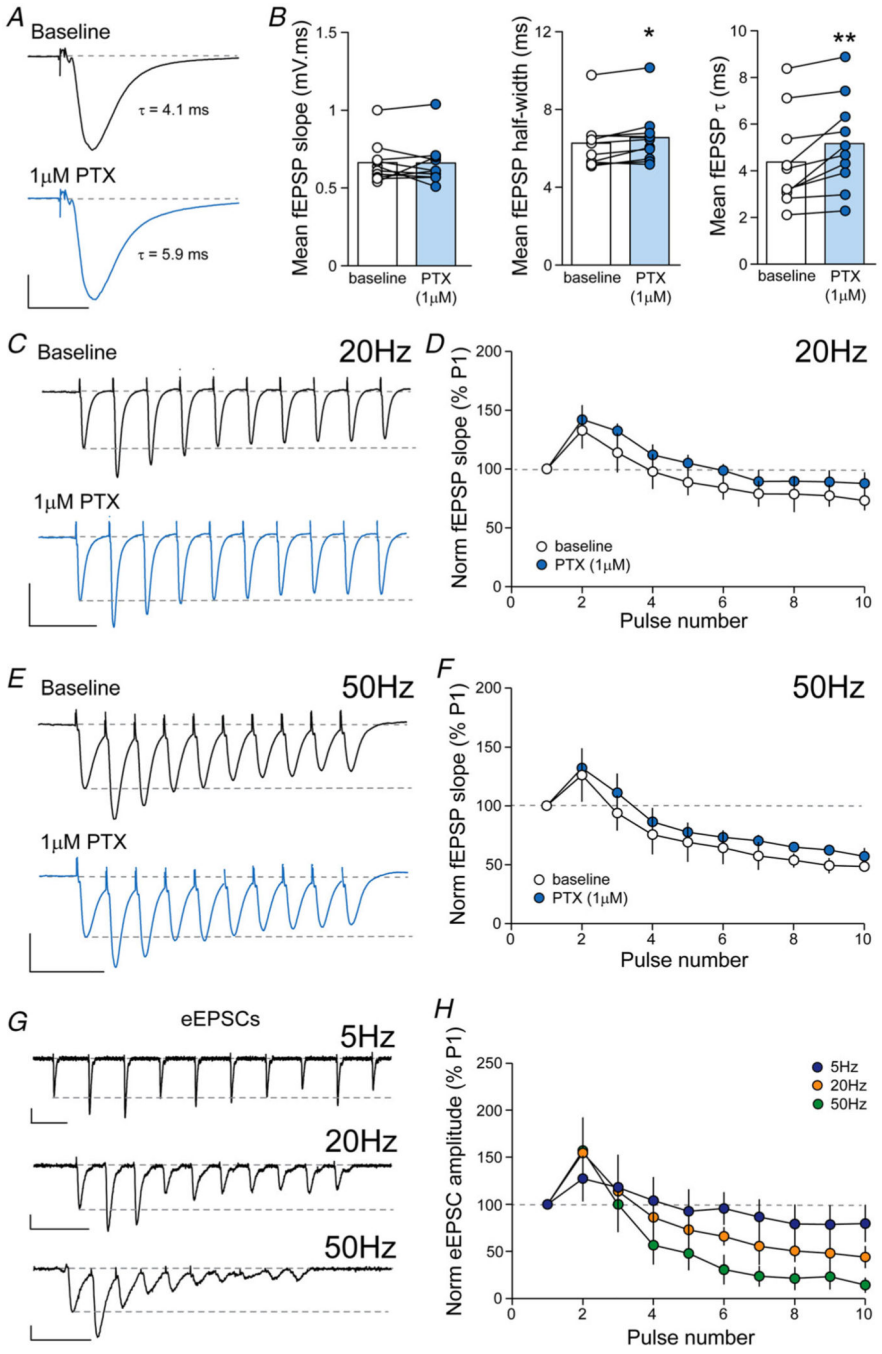

Figure 3. The LPP–DG low pass filter is not dependent upon GABAergic inhibition

A, ensemble averages of LPP fEPSPs recorded from a representative slice in the absence (top) and presence (bottom) of picrotoxin (PTX; 1 μM) (scale bars: $y = 0.5$ mV, $x = 10$ ms). *B*, summary graphs showing the effect of PTX on the mean slope, half-width and decay τ of the LPP fEPSPs. Note that PTX significantly increased the fEPSP duration and decay time (*$P = 0.012$; **$P = 0.007$; baseline *vs.* PTX, paired Student's *t*-test; $n = 10$ slices/5 mice). *C*, representative traces recorded from the DG OML with stimulation (10 pulses) of the LPP at 20 Hz before (black) and after (blue) PTX infusion (scale bars: $y = 1$ mV, $x =$

100 ms). *D*, graph showing the within-train facilitation of the fEPSP slope with 20 Hz LPP stimulation in the absence and presence of bath PTX (**P* = 0.049, $F_{(9,36)}$ = 2.167; two-way RM-ANOVA pulse number *vs*. PTX; *n* = 5 slices/2 mice). *E*, representative traces showing fEPSP responses to LPP stimulation (10 pulses) at 50 Hz before (black) and after (blue) bath application of PTX (scale bars: *y* = 1 mV, *x* = 50 ms). *F*, graph showing the within-train facilitation of the fEPSP slope with 50 Hz LPP stimulation in the absence and presence of PTX (*P* = 0.371, $F_{(9,36)}$ = 1.125 two-way RM-ANOVA pulse number *vs*. PTX; *n* = 5 slices/2 mice). *G*, representative eIPSCs recorded from an exemplar granule cell in response to LPP stimulation at 5, 20 and 50 Hz (scale bars: *y* = 50 pA, *x* = 200 ms, 100 ms and 50 ms). *H*, graph showing the within-train facilitation of the eEPSC for each stimulation frequency (*n* = 7 cells/frequency/4 mice).

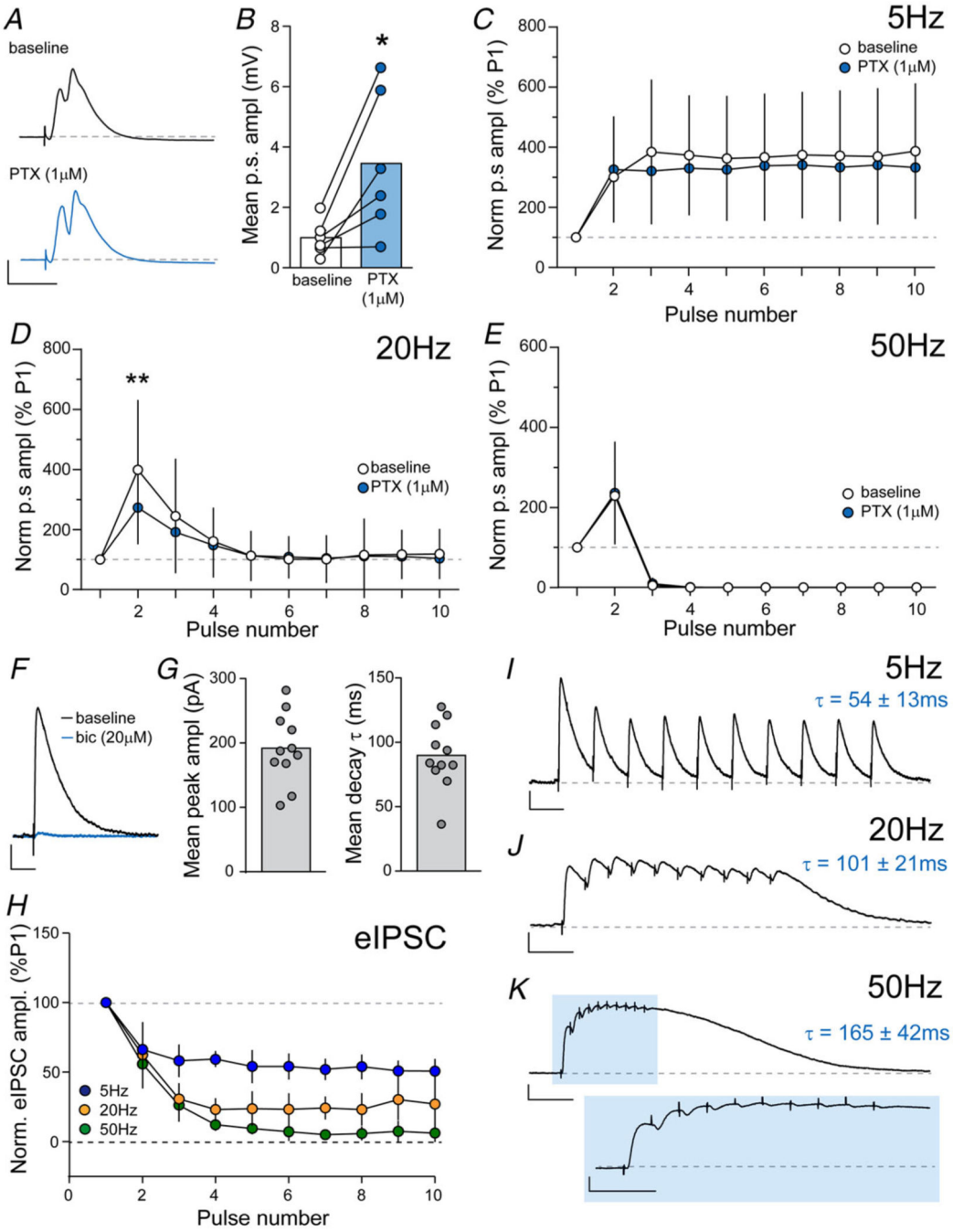

Figure 4. GABAergic inhibition does not shape granule cell output with LPP activation at θ, β and γ frequencies

A, ensemble average LPP-evoked fEPSP recorded from a representative slice in the absence (black) and presence (blue) of picrotoxin (PTX) showing an increase in population spike (p.s.) amplitude with PTX infusion (scale bars: $y = 1$ mV, $x = 10$ ms). *B*, bar graph summarizing the mean population spike amplitude before (white) and following (blue) PTX infusion ($t_5 = 3.10$, $P = 0.027$, $n = 6$ slices/4 mice; paired Student's *t*-test). *C*, plot of DG normalized population spike amplitude across a 10-pulse, 5 Hz train, showing that the facilitation of response amplitude is unaffected by PTX ($F_{(9,54)} = 0.9938$, $P = 0.4562$; two-

way RM-ANOVA; $n = 7$ slices/4 mice). *D*, at 20 Hz, PTX infusion significantly decreased amplitude of DG population-spike elicited by the second pulse only of a 10 pulse train ($F_{(9,45)} = 3.392$, $^{**}P = 0.001$, $n = 6$ slices/4 mice). *E*, PTX did not influence population spike responses to a 10-pulse, 50 Hz train; in both cases there was no detectible population spike by pulse 4 ($F_{(9,45)} = 0.0231$, $P > 0.999$, $n = 7$ slices/4 mice). *F*, representative eIPSCs recorded from an exemplar dentate gyrus granule cell in response to stimulation of the LPP. Bath application of bicuculline (bic; blue) completely blocked the evoked response (scale bars: $y = 50$ pA, $x = 100$ ms). *G*, bar graphs summarizing the mean peak amplitude and decay time) of eIPSCs recorded from dentate gyrus granule cells. *H*, graph summarizing the normalized within-train suppression of eIPSC amplitude in response to stimulation at 5, 20 and 50 Hz frequencies ($n = 7$ cells/4 mice). Note that suppression of the eIPSC although evident at all frequencies shows frequency-dependence. *I–K*, representative eIPSCs recorded from an exemplar dentate gyrus granule cell in response to stimulation of the LPP at 5 Hz (*I*), 20 Hz (*J*) and 50 Hz (*K*). The evoked responses to 50 Hz stimulation are illustrated on an expanded time scale. Scale bars: 5 Hz: $y = 50$ pA, $x = 200$ ms; 20 Hz: $y = 100$ pA, $x = 100$ ms; 50 Hz: $y = 100$ pA, $x = 100$ ms (top) and 50 ms (bottom).

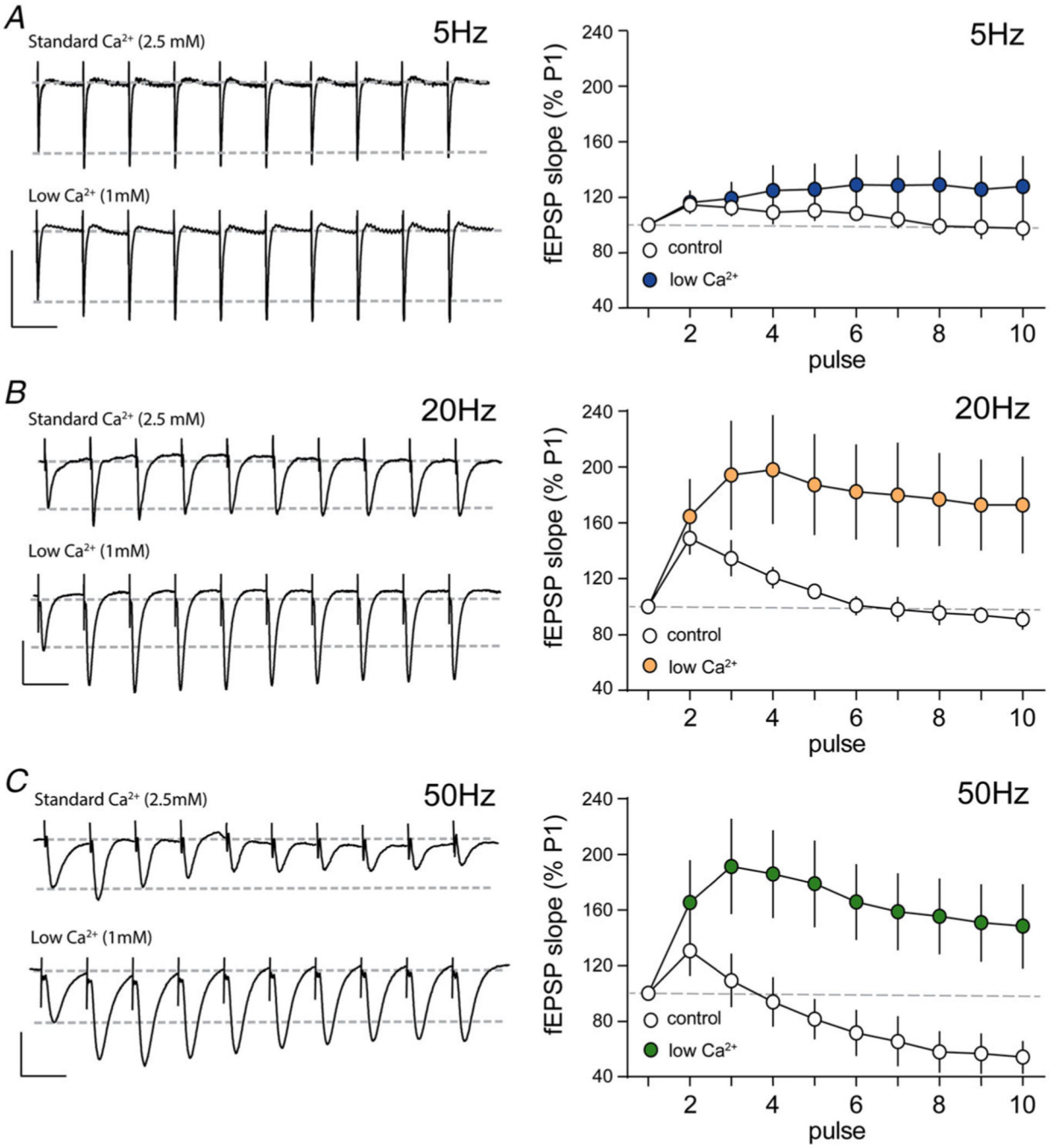

Figure 5. The low pass filter at the LPP–DG synapse is removed by reducing release probability

Representative traces showing LPP responses to stimulation trains (10 pulses) delivered at θ (5 Hz) (*A*), β (20 Hz) (*B*) and γ (50 Hz) (*C*) frequencies under high (2.5 mM; top) and low (1 mM; bottom) Ca^{2+} conditions. Corresponding line graphs (right) illustrate the nature of within-train facilitation and suppression under the different Ca^{2+} conditions (n = 7–12 slices/group; n = 4–5 mice/group). Note the marked increase in facilitation, particularly at higher stimulation frequencies, when external Ca^{2+} is reduced. Scale bars: 5 Hz: y = 1 mV, x = 200 ms; 20 Hz: y = 1 mV, x = 50 ms; 50 Hz: y = 1 mV, x = 20 ms.

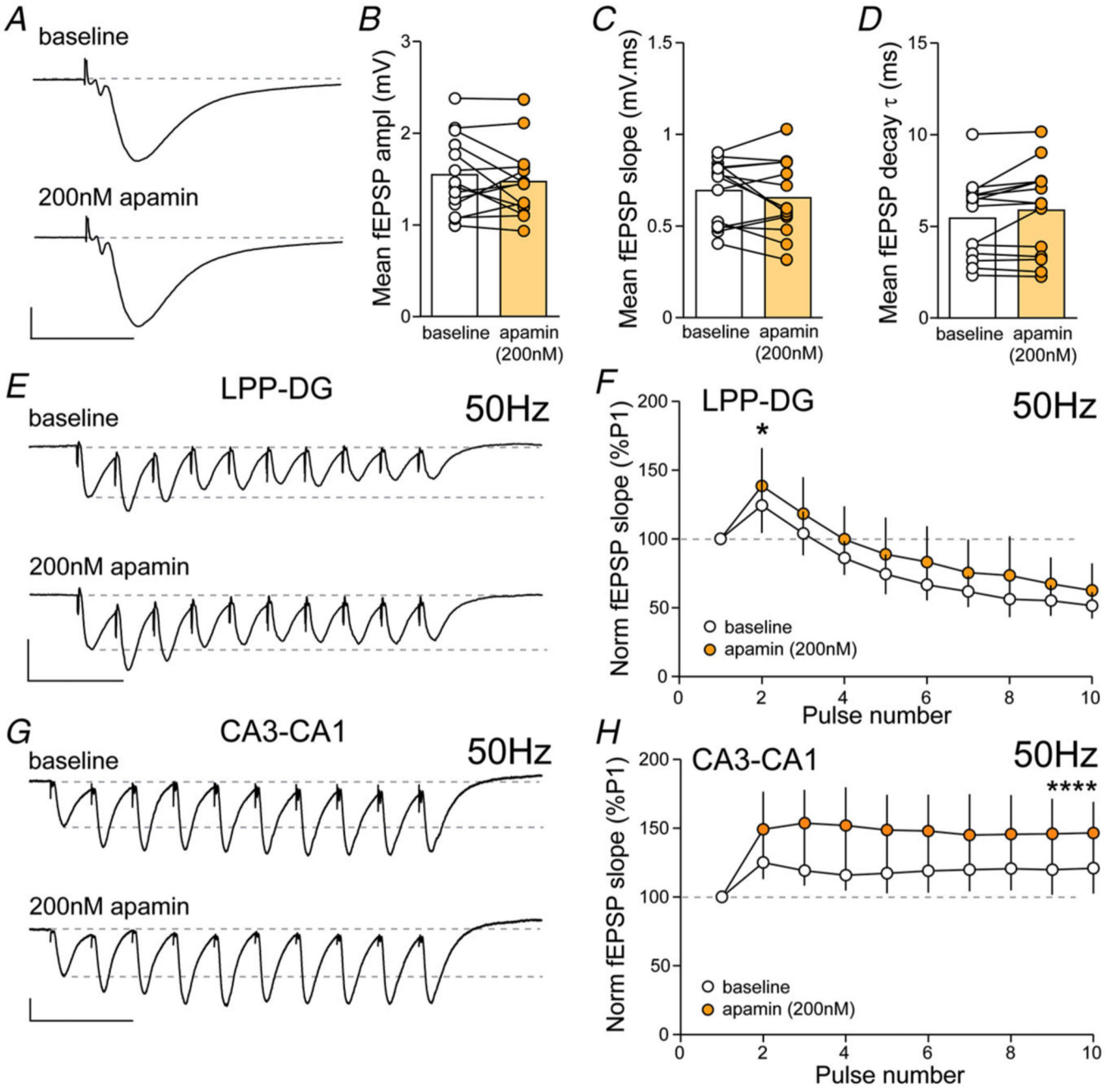

Figure 6. The LPP–DG low pass filter does not require activation of Ca^{2+}-dependent SK channels

A, ensemble averages of fEPSPs recorded from a representative slice in the absence (top) and presence (bottom) of the SK channel antagonist apamin (200 nM; scale bars: $y = 0.5$ mV, $x = 10$ ms). *B–D*, graphs showing the effect of apamin upon the mean amplitude (*B*), slope (*C*) and decay τ (*D*) of LPP-evoked fEPSPs (bars show group means; points show individual slice measures). Apamin had no significant effect on any of the fEPSP parameters (amplitude: $P = 0.309$; slope: $P = 0.267$; τ: $P = 0.053$ baseline *vs.* apamin; paired Student's *t*-test; $n = 14$ slices/7 mice). *E*, representative traces showing LPP responses to 10 pulse

stimulation trains delivered at 50 Hz before (top) and after (bottom) apamin infusion (scale bars: $y = 1$ mV; $x = 50$ ms). *F*, graph summarizing the within-train facilitation of fEPSP slope with and without apamin present. The inhibitor significantly increased facilitation only during the second pulse (*$P = 0.027$ at pulse 2, $F_{(9,63)} = 2.290$ two-way RM-ANOVA, $n = 8$ slices/4 mice). *G*, representative traces showing fEPSP responses to field CA3–CA1 Schaffer-commissural stimulation at 50 Hz (10-pulse trains) before (top) and after (bottom) apamin infusion. *H*, the within-train facilitation was enhanced 40 min after apamin infusion onset through the duration of the train ($F_{(9,54)} = 4.67$, $^{****}P < 0.0001$; $n = 7$ slices/5 mice; two-way RM-ANOVA).

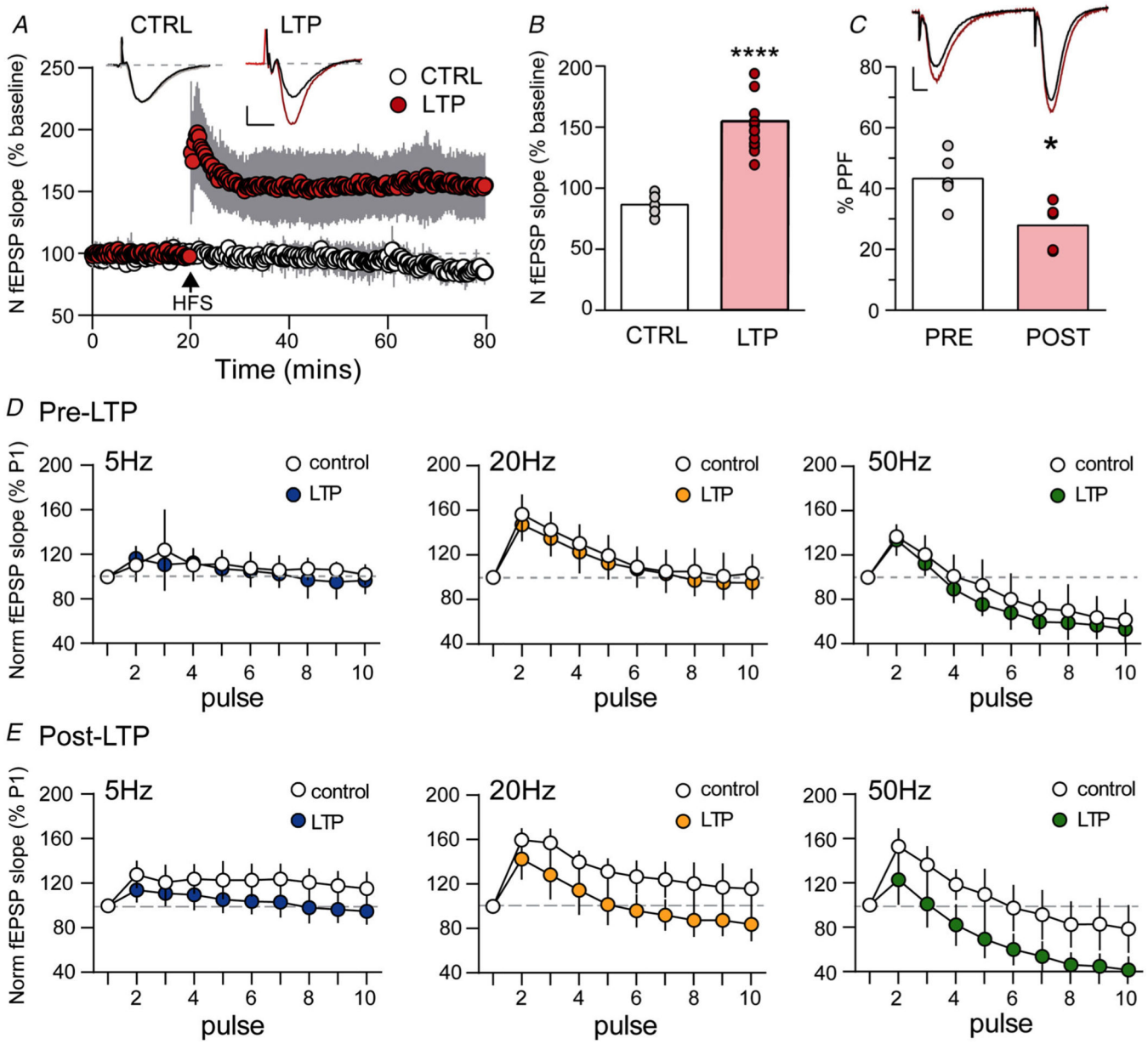

Figure 7. LTP modifies synaptic filtering at the LPP–DG synapse

A, LTP was induced in the LPP–DG synapses via high frequency stimulation (HFS, at upward arrow) that resulted in a 50% increase in response compared to slices that did not receive HFS. Representative traces show LPP responses before and 60 min after HFS (right) or control low frequency stimulation (left) (scale bars: $y = 0.5$ mV, $x = 5$ ms) ($n = 12$ slices/7 mice). *B*, the mean response (fEPSP slope) recorded 55–60 min post-HFS, normalized to same-slice baseline, was markedly potentiated relative to similarly normalized measures from control slices ($t_{(17)} = 6.14$, ****$P < 0.0001$, paired *t*-test of the average of the last 5 min). *C*, top: representative traces of paired-pulse stimulation of the LPP–DG (40 ms between pulses) before (black) and 60 min after (red) LPP-LTP induction. Bottom: PPF of the fEPSP slope was reduced 60 min after inducing LPP-LTP relative to baseline levels (t_4

= 3.02, n = 5 slices/3 mice, *P = 0.039; scale bars: y = 0.5 mV, x = 5 ms). *D*, responses to trains of 5, 20 and 50 Hz stimulation applied to the LPP before HFS (or control LFS) reveal no differences between the groups (5 Hz: $F_{(9,135)}$ = 1.85, P > 0.05; 20 Hz: $F_{(9,153)}$ = 0.75, P > 0.05; 50 Hz: $F_{(9,135)}$ = 1.56, P > 0.05; two-way RM-ANOVA). *E*, responses to stimulation trains applied to the LPP 45–60 min after LTP induction revealed striking differences in the pattern of frequency facilitation for slices that were potentiated compared to those (control) that were not. At 5 Hz, facilitation is sustained throughout the train in control slices but was absent in slices that had been potentiated (interaction between pulse number and groups: $F_{(9,162)}$ = 5.41, ****P < 0.0001). The frequency facilitation profiles are also significantly different between control and LTP slices in response to 20 Hz stimulation (interaction $F_{(9,153)}$ = 5.78, ****P < 0.0001) and 50 Hz ($F_{(9,135)}$ = 5.85, ****P < 0.0001). For all panels n = 11 slices/7 mice, unless otherwise specified.

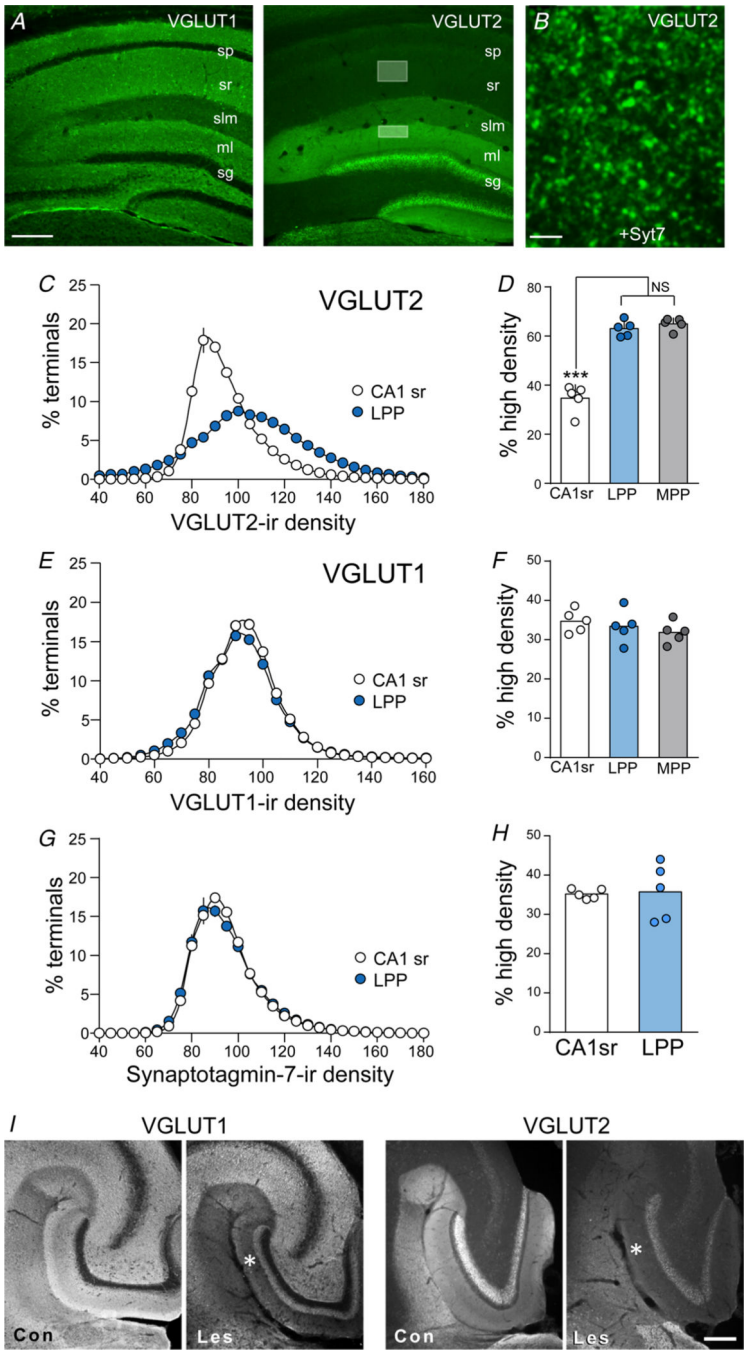

Figure 8. VGLUT2 is selectively concentrated in LPP terminals

A, representative photomicrographs of VGLUT1- and VGLUT2-immunoreactivity (ir) in mouse hippocampal subfields. The shaded boxes illustrate the sample fields used for FDT analyses of terminals in the DG OML for the LPP and CA1 stratum radiatum (sr) for CA3–CA1 terminals. Calibration bar, 200 μm. ml, molecular layer of the DG; sg, stratum granulosum; slm, stratum lacunosum-moleculare; sp, stratum pyramidale. *B*, photomicrograph of VGLUT2-ir in the LPP field. Inset shows double-labelling for both VGLUT2 (green) and Syt7 (red) in the LPP field; double-labelled profiles are seen as either

touching or overlapping (yellow). Calibration bar, 1 μm; 0.6 μm for inset. *C*, intensity frequency distribution curves for VGLUT2-ir in Syt-7 positive terminals in CA1 sr and the LPP ($F_{(50,400)}$ = 63.52; ***P < 0.0001; n = 5 mice/group); plots show group mean ± SEM values throughout (note, some error bars are short and covered by symbols for panels *C*, *E* and *G*). *D*, bar graph showing there is a greater percentage of terminals with high density VGLUT2-ir in the LPP field as compared to CA1 sr ($F_{(2,12)}$ = 84.56, P < 0.0001; one-way AVOVA; ***P < 0.0001, Tukey's test; high density is ≥ 100 in *C* and *E*). Note that percentage of synapses with high density VGLUT2-ir is not significantly different between the LPP and MPP fields (P = 0.558, Tukey's test). *E*, intensity frequency distribution curves for VGLUT1-ir in Syt-7 positive presynaptic terminals in CA1 sr and the LPP ($F_{(31,248)}$ = 5.533; ***P < 0.0001; n = 5 mice/group). *F*, bar graph showing the percentage of terminals with high density (≥100) levels of VGLUT1-ir ($F_{(2,12)}$ = 1.056, P = 0.3781). *G*, intensity frequency distribution curves for Syt7-ir in CA1 sr and the LPP ($F_{(50,400)}$ = 1.358; P = 0.0602). *H*, bar graph showing the percentage of terminals with high density (≥100) levels of Syt7-ir (P = 0.8859; paired Student's t-test). *I*, photomicrographs of VGLUT1-ir and VGLUT2-ir in the DG molecular layer ipsilateral to an entorhinal cortex lesion (Les) and on the contralateral, control (Con) side; asterisks denote the loss of immunolabelling in the perforant path terminal fields. Calibration bar, 200 μm.

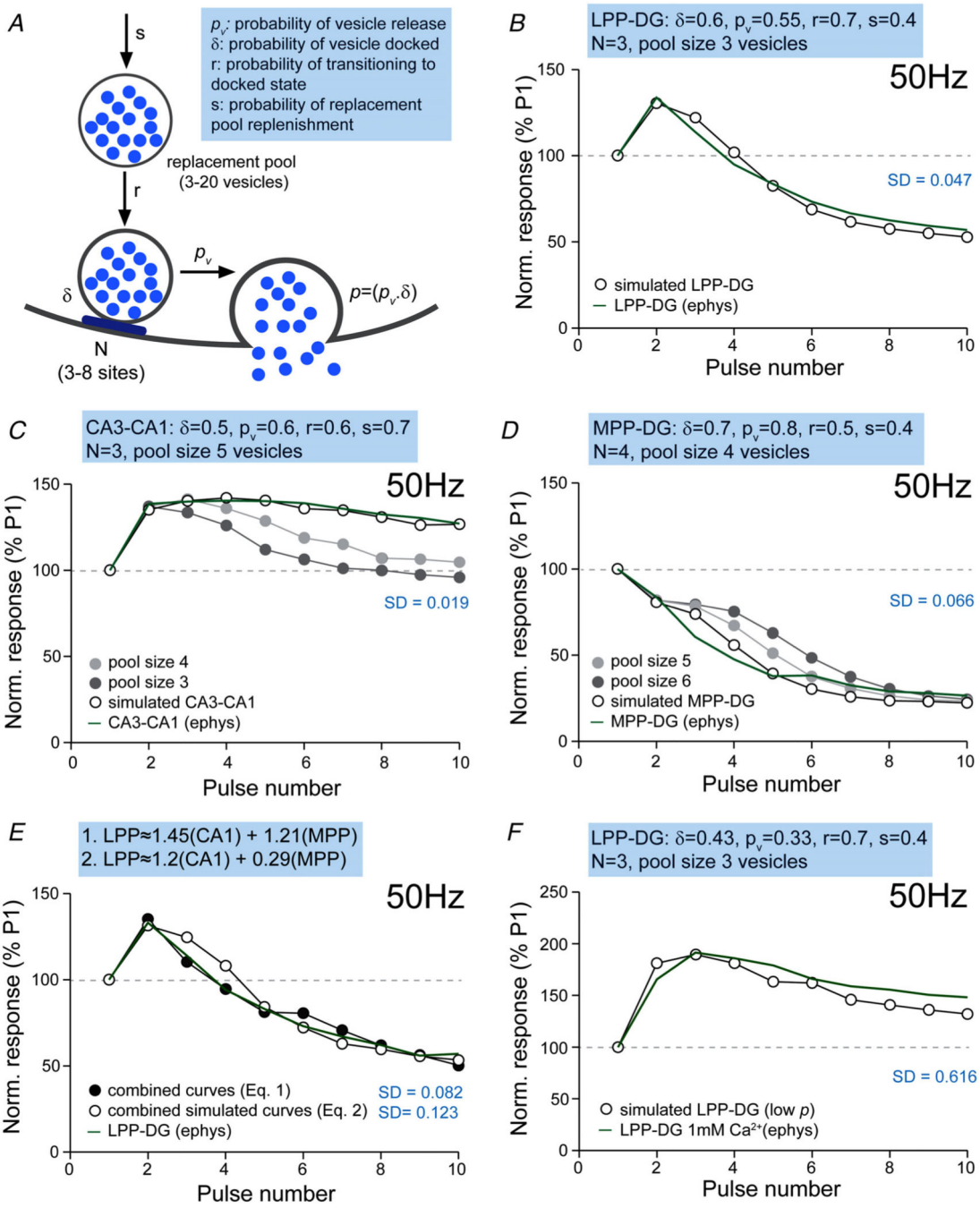

Figure 9. Monte Carlo simulations of a two-step release model recapitulate the output curves across three different types of synapse

A, schematic illustration of the variables within the two-step model where N represents the number of docking sites. *B*, using physiologically constrained parameters, the two-step model (white circles) reliably recapitulates the electrophysiologically recorded responses (green line) following γ frequency stimulation of the LPP. When constrained by initial *p*, the two-step model reliably recapitulates the low-*p* CA3–CA1 synapse (*C*) and high-*p* MPP–DG synapse (*D*). Note that the simulated output at both of these synapses was highly sensitive to the pool size. *E*, the LPP–DG output curve (green line) could be replicated by

combining either the simulated (white circles) or empirically measured (black circles) CA3–CA1 and MPP–DG curves when weighted appropriately. The equations used to generate each curve are given above. *F*, reducing the initial *p* prevented the simulated within-train suppression of responses (white circles), producing an output curve similar to that recorded electrophysiologically under conditions of low external Ca^{2+} (green line).

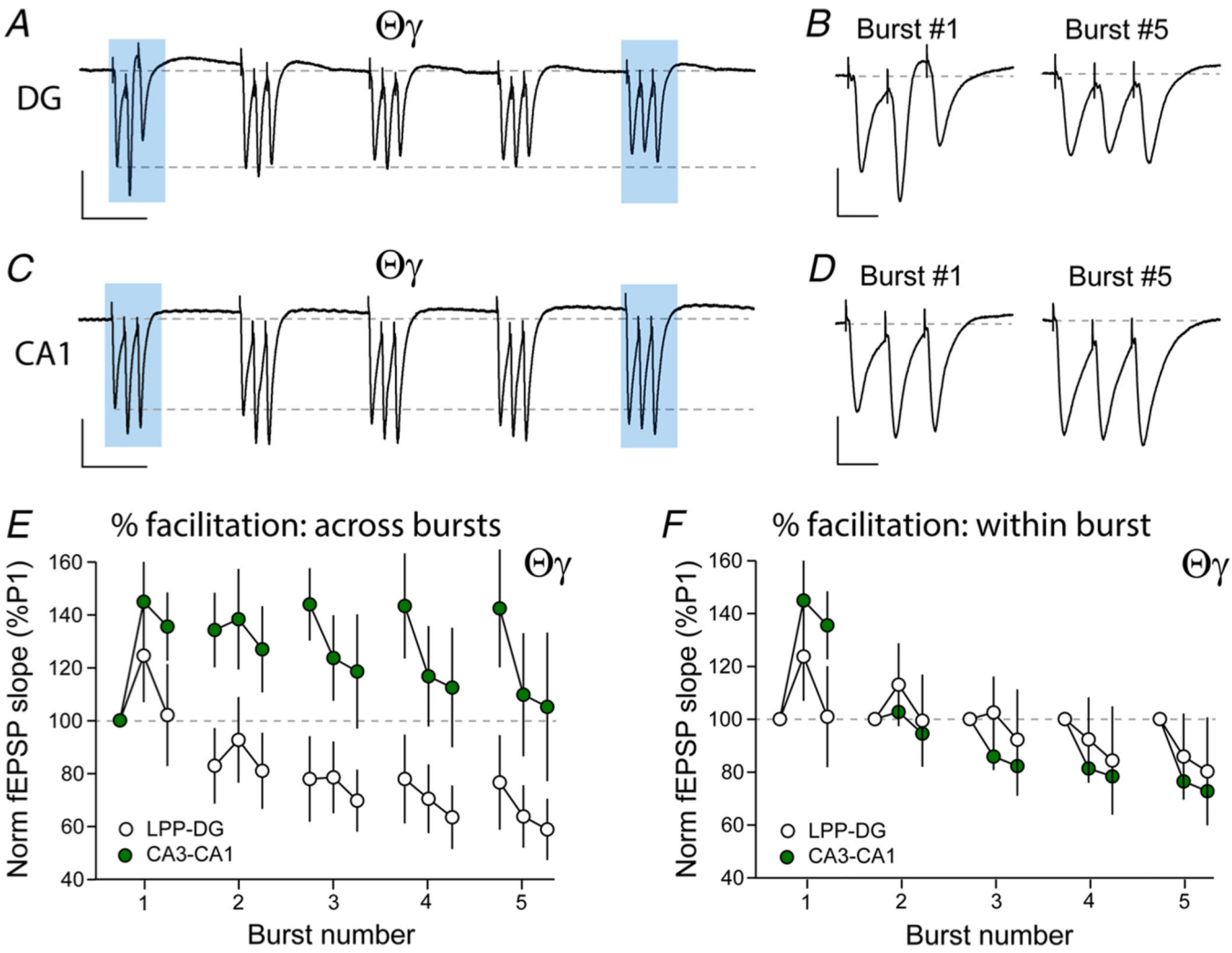

Figure 10. Processing short bursts of γ frequency information occurs differently at LPP–DG and CA3–CA1 synapse

Representative traces recorded from the OML of the DG (*A* and *B*) and str. radiatum of CA1 (*C* and *D*) in response to five γ frequency bursts (three pulses) delivered at intervals of 200 ms (i.e. $\theta\gamma$) via the LPP and Schaffer–commissural (CA3–CA1) projections, respectively (LPP–DG: $n = 39$ slices/13 mice; CA3–CA1: $n = 7$ slices/4 mice). The responses to pulse 1 and pulse 5 (shaded areas) are illustrated on an expanded time scale for LPP–DG (*B*) and CA3–CA1 (*D*); scale bars: $y = 1$ mV, $x = 100$ ms (*A* and *C*) or 20 ms (*B* and *D*). *E*, graph summarizing the change in fEPSP slopes (relative to the initial response of the first burst) during $\theta\gamma$ stimulation (five bursts) at LPP–DG and CA3–CA1 synapses. Note that CA3–CA1 exhibit facilitation that is maintained across successive bursts whereas suppression occurs at LPP–DG synapses. *F*, graph summarizing the decline in within-burst facilitation that occurs across successive bursts delivered at $\theta\gamma$ patterns at CA3–CA1 and LPP–DG synapses. Other than the marked difference in facilitation of the first burst, both synapses show a similar decline across successive bursts.

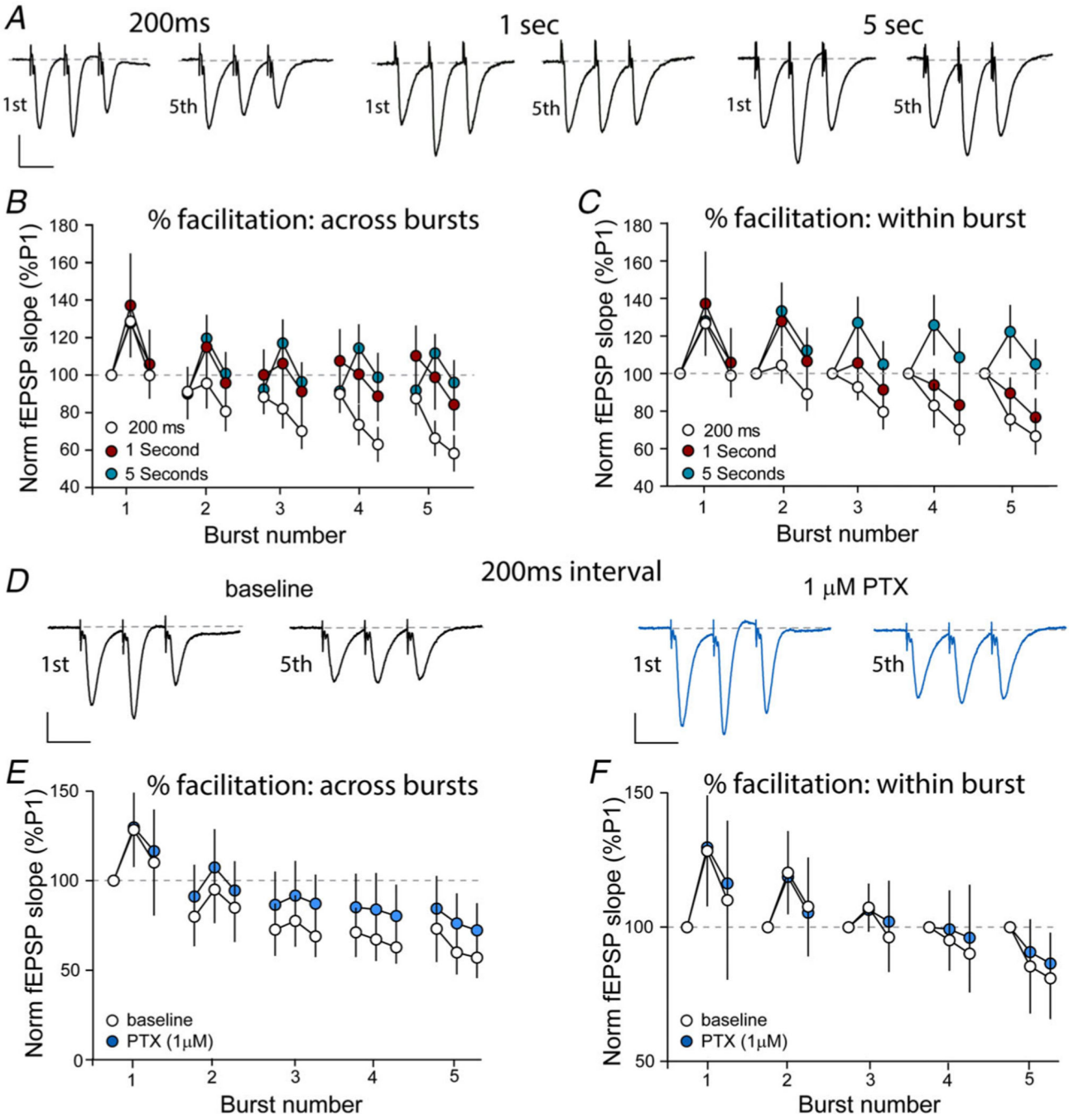

Figure 11. Suppression of within-burst facilitation persists for a prolonged period and does not involve enhanced $GABA_AR$-mediated inhibition

A, representative responses of the LPP to the first and fifth burst recorded from the OML of the DG evoked during a train of five γ frequency bursts (three pulses) delivered to the LPP with intervals of 200 ms, 1 s and 5 s (scale bars: $y = 0.5$ mV, $x = 20$ ms). *B*, graph summarizing the change in fEPSP slopes (relative to the initial response of the first burst) during stimulation of the LPP with γ frequency bursts (five bursts) separated by intervals indicated (200 ms: $n = 19$ slices/8 mice; 1 s: $n = 11$ slices/5 mice; 5 s: $n = 14$ slices/3 mice). *C*, graph summarizing the within-burst facilitation that occurs across successive

bursts delivered at intervals indicated. Note that the within-burst facilitation is maintained when bursts are separated by intervals of 5 s (blue symbols) (200 ms: $n = 19$ slices/8 mice; 1 s: $n = 11$ slices/5 mice; 5 s: $n = 14$ slices/3 mice). *D*, representative responses to the first and fifth burst recorded from the OML evoked during a train of five γ frequency bursts (three pulses) delivered to the LPP at intervals of 200 ms before (black) and after (blue) bath application of PTX (scale bars: $y = 0.5$ mV, $x = 20$ ms). *E*, graph summarizing the change in fEPSP slopes (relative to the initial response of the first burst) during $\theta\gamma$ stimulation (five bursts) before (white circle) and after (blue circle) bath application of PTX. Treatment with PTX results in a modest enhancement of responses across bursts ($F_{(14,112)} = 1.964$, $P = 0.0269$; $n = 9$ slices/4 mice per group; two-way RM-ANOVA). *F*, Graph showing the similar decline in within-burst facilitation that occurs across successive bursts delivered at $\theta\gamma$ patterns before (white circle) and after (blue circle) PTX ($F_{(14,112)} = 0.5098$, $P = 0.9232$; $n = 9$ slices/4 mice per group; two-way RM-ANOVA).

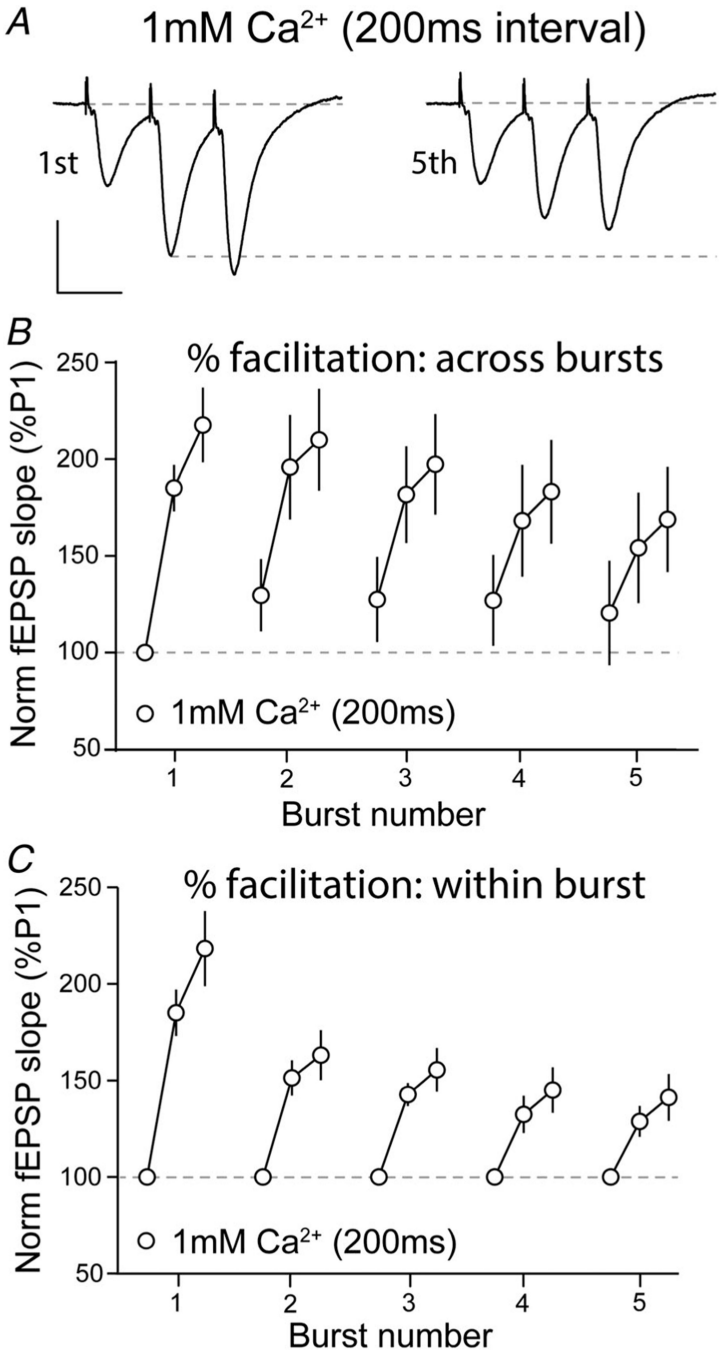

Figure 12. Reducing the initial release probability (*p*) removes the filter associated with brief γ frequency bursts at the LPP–DG synapse

A, representative responses to the first and fifth burst recorded in low Ca^{2+} (1 mM) aCSF from the OML of the DG evoked during a train of five γ frequency bursts (three pulses) delivered to the LPP at intervals of 200 ms (scale bars: $y = 0.5$ mV, $x = 20$ ms). *B*, graph summarizing the change in fEPSP slopes (relative to the initial response of the first burst) during $\theta\gamma$ stimulation (five bursts, 200 ms interval) under low external Ca^{2+} ($n = 8$ slices/4 mice). *C*, graph summarizing the within-burst facilitation that occurs across successive bursts delivered at $\theta\gamma$ patterns. Under low external Ca^{2+}, both initial response

and within-burst facilitation is maintained across bursts, although the latter declines across successive bursts (n = 8 slices/4 mice).

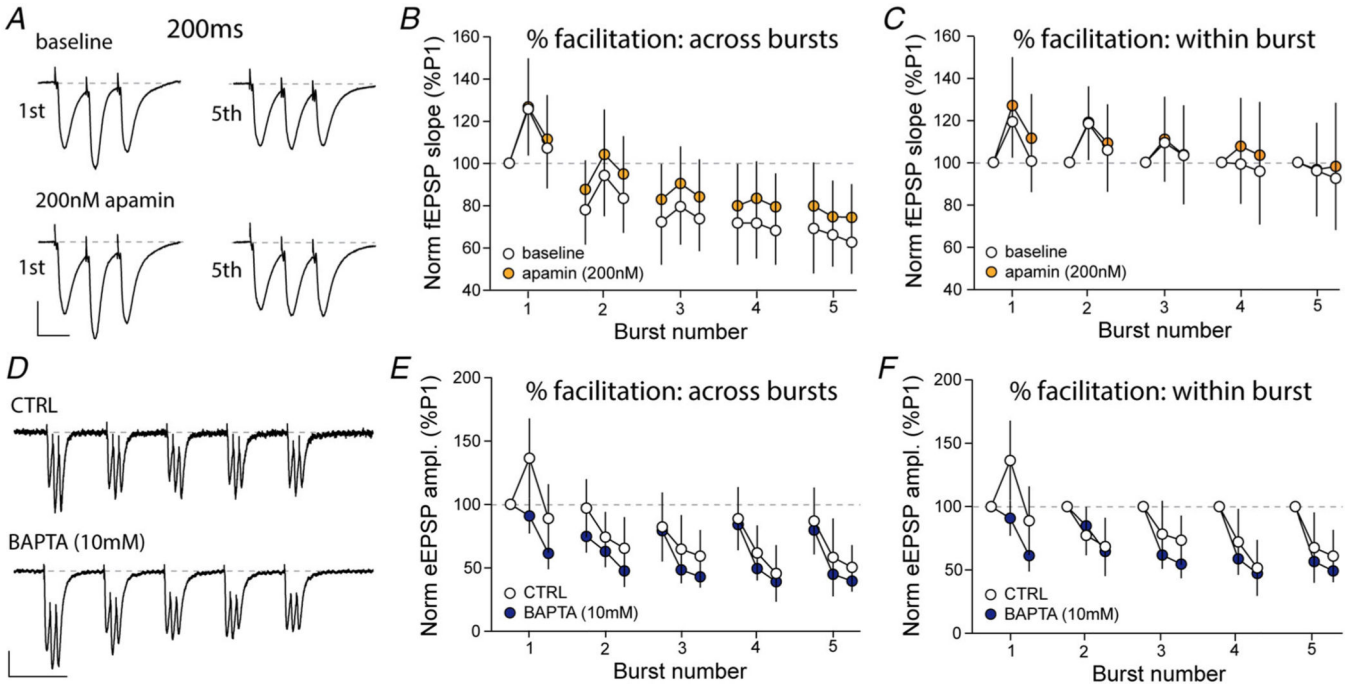

Figure 13. Postsynaptic Ca^{2+}-dependent mechanisms do not contribute to the prolonged suppression of within burst facilitation

A, representative responses to the first and fifth burst recorded from the DG OML evoked during a train of five γ frequency bursts (three pulses) delivered to the LPP at intervals of 200 ms before (top) and during (bottom) bath application of the SK channel antagonist apamin (200 nM; scale bars: $y = 0.5$ mV, $x = 20$ ms). *B*, graph summarizing the change in fEPSP slopes (relative to the initial response of the first burst) during $\theta\gamma$ stimulation (five bursts) before (white circle) and after (orange circle) bath application of apamin. Apamin caused a modest enhancement of responses across bursts ($F_{(14,182)} = 2.459$, $P = 0.003$; $n = 13$ slices/4 mice; two-way RM-ANOVA). *C*, graph summarizing the decline in within-burst facilitation that occurs across successive bursts delivered at $\theta\gamma$ patterns before (white circle) and with (orange circle) apamin present. Note the marked decline in the within-burst facilitation occurring across bursts during $\theta\gamma$ stimulation is modestly enhanced by apamin ($F_{(14,182)} = 1.873$, $P = 0.032$; $n = 13$ slices/4 mice; two-way RM-ANOVA). *D*, exemplar eEPSCs recorded from DG granule cells following $\theta\gamma$ stimulation of the LPP without (top) and with (bottom) the Ca^{2+} chelator BAPTA in the electrode's internal solution (scale bars: $y = 50$ pA, $x = 200$ ms). *E* and *F*, graphs summarizing the relative change in the amplitude of eEPSC across bursts (*E*), and the decline in within-burst facilitation (*F*) that occurs following the activation of the LPP with $\theta\gamma$ patterns of input. Note that BAPTA does not attenuate these responses (CTRL: $n = 7$ cells; BAPTA: $n = 4$ cells/3−4 mice).

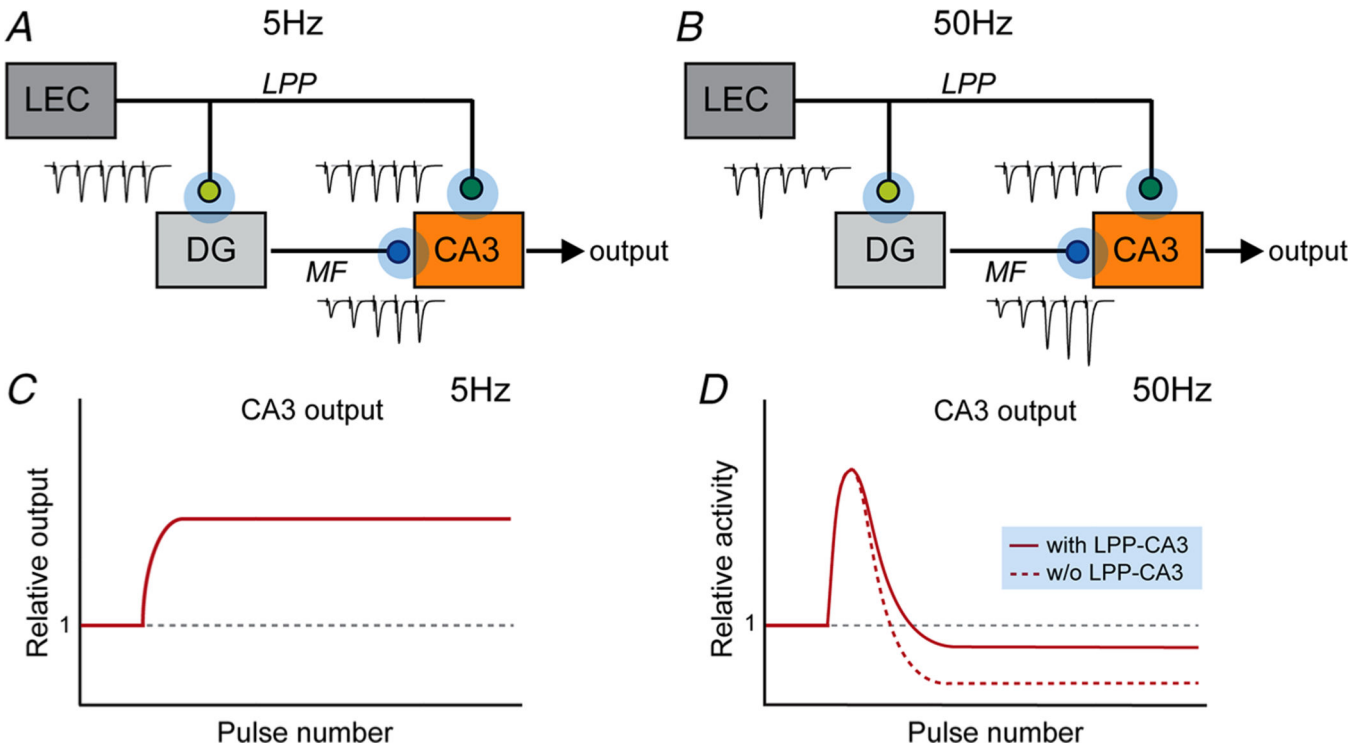

Figure 14. Schematic representation of direct and indirect inputs to CA3 with predicted outputs to activation at 5 Hz and 50 Hz

A and *B*, schematic illustration of the proposed responses at the LPP–DG (yellow), LPP–CA3 (green) and Mossy Fiber (MF)–CA3 synapses in response to afferent inputs firing at 5 Hz (*A*) and 50 Hz (*B*). LEC, lateral entorhinal cortex. *C* and *D*, graphs depicting the predicted output (red) from field CA3 following activation at 5 Hz (*C*) and 50 Hz (*D*) based upon the synaptic transformations that occur across the three synapses within the circuit at each frequency. At 5 Hz modest frequency facilitation at both LPP–DG and LPP–CA3 synapses is accompanied by pronounced facilitation of responses at the MF–CA3 synapse (*A*). However, the predicted CA3 output (*C*) is not simply the sum of the facilitation across the three synapses as the MF–CA3 preferentially promotes robust feed-forward inhibition via activation of the interneuron network at 5 Hz. As such, one would predict that feed-forward inhibition will dampen the output from CA3. At higher stimulation frequencies (50 Hz), the output from CA3 will be largely determined by the balance between suppression of responses at the LPP–DG synapse and the robust frequency facilitation occurring at the MF–CA3. In *D*, the hypothetical outputs with and without a contribution from the direct LPP–CA3 input is shown. We propose that at γ frequencies (i.e. 50 Hz) activation of the LPP–CA3 will, due to its ability to largely follow inputs in this frequency range, increase the CA3 output. One should note that the proposed model does not account for the manner in which different frequencies of afferent stimulation may shape output from CA3 such that throughput is enhanced or suppressed.